

1 **TITLE:**
2 A shift from pleiotropic to modular adaptation revealed by a high-resolution two-step adaptive
3 walk

4
5 **AUTHORS:**
6 Grant Kinsler^{1,2}, Yuping Li^{3,4}, Gavin Sherlock^{*3}, Dmitri A. Petrov^{*1}

7
8 **AFFILIATIONS:**
9 ¹Department of Biology, Stanford University
10 ²Department of Bioengineering, University of Pennsylvania
11 ³Department of Genetics, Stanford University
12 ⁴Department of Microbiology & Immunology, UC San Francisco
13 *Equal contribution

14
15 **ABSTRACT:**
16
17 Evolution by natural selection is expected to be a slow and gradual process. In particular, the
18 mutations that drive evolution are predicted to be small and modular, incrementally improving a
19 small number of traits. However, adaptive mutations identified early in microbial evolution
20 experiments, cancer, and other systems often provide substantial fitness gains and
21 pleiotropically improve multiple traits at once. We asked whether such pleiotropically adaptive
22 mutations are common throughout adaptation or are instead a rare feature of early steps in
23 evolution that tend to target key signaling pathways. To do so, we conducted barcoded second-
24 step evolution experiments initiated from five first-step mutations identified from a prior yeast
25 evolution experiment. We then isolated hundreds of second-step mutations from these evolution
26 experiments, measured their fitness and performance in several growth phases, and conducted
27 whole-genome sequencing of the second-step clones. Here, we found that while the vast
28 majority of mutants isolated from the first-step of evolution in this condition show patterns of
29 pleiotropic adaptation - improving both performance in fermentation and respiration growth
30 phases - second-step mutations show a shift towards modular adaptation, mostly improving
31 respiration performance and only rarely improving fermentation performance. We also identified
32 a shift in the molecular basis of adaptation from genes in cellular signaling pathways towards
33 genes involved in respiration and mitochondrial function. Our results suggest that the genes in
34 cellular signaling pathways are particularly capable of providing large, adaptively pleiotropic
35 benefits to the organism due to their ability to coherently affect many phenotypes at once. As
36 such, these genes may serve as the source of pleiotropic adaptation in the early stages of
37 evolution, and once these become exhausted, organisms then adapt more gradually, acquiring
38 smaller, more modular mutations.

39 **INTRODUCTION**

40
41 As organisms adapt to their environment, they face a multi-dimensional optimization problem.
42 To be advantageous, new mutations must improve one or more traits under selection without
43 imposing strong costs on other traits. Theoretical analyses of adaptive walks in multi-
44 dimensional trait spaces suggest that mutations that generate small phenotypic shifts in few
45 traits are more likely to be beneficial overall than mutations of large phenotypic effect on many
46 traits (Orr 2000). Consequently, adaptive mutations are expected to both provide small fitness
47 benefits and to be **modular** – that is, affect only a few traits without affecting others.

48
49 Despite these theoretical expectations, microbial evolution experiments have revealed that early
50 adaptation often proceeds by single mutations that provide large fitness benefits (Y. Li, Petrov,
51 and Sherlock 2019; Wiser, Ribeck, and Lenski 2013; Levy et al. 2015; Johnson et al. 2021;
52 Venkataram et al. 2016). Moreover, in the cases where the improvement of these mutations has
53 been decomposed into distinct trait performances, it is often observed that these mutations
54 improve multiple traits simultaneously (as illustrated in Figure 1A) (Y. Li, Petrov, and Sherlock
55 2019; Y. Li et al. 2018; Bono et al. 2017; Jasmin and Kassen 2007).

56
57 The observation of adaptive mutations improving multiple performances at once, which we here
58 term “**pleiotropic adaptation**”, can be easily seen in a series of evolution experiments
59 conducted with barcoded yeast in which a comprehensive set of adaptive mutations was
60 profiled for their effects on likely orthogonal trait performances (Levy et al. 2015; Venkataram et
61 al. 2016; Y. Li, Petrov, and Sherlock 2019; Y. Li et al. 2018). Li et al (2018) in particular showed
62 that ~85% of first-step adaptive mutations isolated from their evolution experiment improve
63 performance in both fermentation and respiration growth phases, both of which are under
64 selection during the yeast growth cycle. These pleiotropic mutants from this initial step of
65 adaptation, many of which harbor only a single mutation in the Ras/PKA pathway, are also
66 strongly adaptive, providing fitness benefits of up to 120% per growth cycle (roughly 15% per
67 generation) (Venkataram et al. 2016). Such large-effect Ras/PKA pathway mutations are
68 commonly found in early evolution in other systems, such as cancer progression (Bailey et al.
69 2018). As the study we present here follows on from our previous series of findings, we use
70 these yeast mutations as a motivating example throughout the rest of the introduction.

71
72 How do we reconcile our observations of pleiotropic adaptation (Y. Li et al. 2018) with
73 theoretical expectations that these mutations should affect only a small number of traits? One
74 possibility is that fermentation and respiration performances are not as distinct as we believe.
75 However, a number of adaptive mutations do improve only one of these performances,
76 demonstrating that it is in fact possible to shift one performance without affecting the other.

77
78 The other possibility is that the Ras/PKA pathway is wired in such a way that mutations that
79 target this pathway are capable of being both pleiotropic and adaptive, affecting many
80 phenotypes of the organism but in a coherent and coordinated fashion. It might be that

81 mutations in general might not have these patterns of pleiotropic adaptation and instead exhibit
82 “**modular adaptation**”, improving only a subset of the traits under selection. Thus, isolating and
83 characterizing the effects of subsequent mutations, which may be less likely to target this
84 already-mutated pathway, might better reflect the pleiotropic properties of adaptive mutations
85 beyond these extremely beneficial first-step mutations in the Ras/PKA pathway. One way in
86 which we can assess whether the observed adaptive pleiotropy is a common feature of adaptive
87 mutations is to conduct adaptive walks, evolving populations further in the same environment.
88 We can then ask whether later adaptive mutations continue to show pleiotropic adaptation or
89 not.

90

91 One possibility is that pleiotropic adaptation is indeed common. This may be true if there are
92 many pathways in the cell that can be mutated to yield simultaneous improvement of the traits
93 under selection or, instead, if the signaling pathways mutated early can continue to be optimized
94 beyond the first adaptive step. In this scenario, second-step adaptive mutations would continue
95 to improve both traits under selection (Figure 1B, red points) and longer adaptive walks would
96 also continue to show this pattern of pleiotropic adaptation (Figure 1B arrows).

97

98 Alternatively, pleiotropic adaptation may be rare, and first-step mutations target the only (or one
99 of few) signaling pathway(s) which can result in simultaneous improvement of multiple traits
100 (performance in both fermentation and respiration growth phases in the case of the yeast
101 evolution experiments). For adaptation to continue, it would need to engage the modules that
102 can independently control the performance in each growth phase. Individual second-step
103 mutations under this scenario would then be expected to exhibit a pattern of “modular
104 adaptation”, improving only one performance under selection or the other (Figure 1C). The
105 longer adaptive walks could continue down this route of specialization in either a single
106 performance (blue or magenta arrows) or instead improve both performances under selection,
107 but via sequential improvement of one performance and then the other (orange arrows).

108

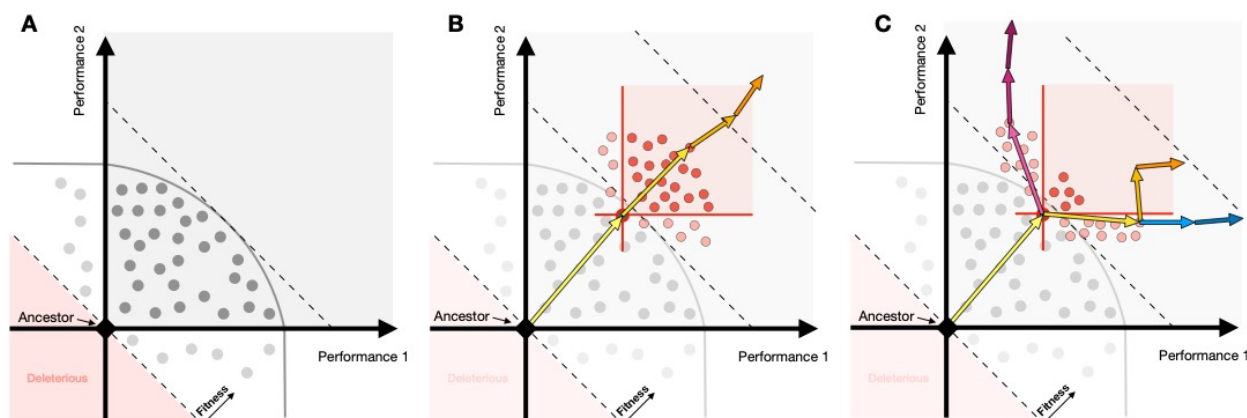
109 Thus, to characterize the nature of single-step adaptive mutations and whether the observation
110 of pleiotropic adaptation of first-step mutations is a general feature of individual adaptation-
111 driving mutations or instead a rare feature of early adaptive mutations, we need to
112 experimentally conduct high-resolution adaptive walks, wherein we can isolate adaptive
113 mutations, quantify their effects on traits relevant to fitness, and identify the molecular basis of
114 adaptation. The yeast barcoding system developed by (Levy et al. 2015) is particularly well-
115 suited for this set of experiments, as we can isolate hundreds of mutations per evolution
116 experiment and study their properties via pooled fitness measurement experiments.

117

118 In this study, we perform second-step evolution experiments using a set of five first-step
119 adaptive mutations isolated from a glucose-limited evolution experiment (Levy et al. 2015) as
120 new ancestors. We then isolate hundreds of mutants from these evolution experiments and
121 measure their performance in the growth phases that make up the evolution condition. We find
122 a shift in the nature of adaptation over this two-step adaptive walk. While first-step mutations

123 primarily demonstrate pleiotropic adaptation, improving performance in both growth phases
 124 under selection, second-step mutations instead primarily exhibit modular adaptation, improving
 125 performance in only a single growth phase under selection (Figure 1C). Whole genome
 126 sequencing reveals an associated shift in the molecular basis of adaptation: from first-step
 127 mutations in general signaling pathways to second-step mutations in genes related to
 128 mitochondrial function and respiration. Finally, we sample rare adaptive clones that showed
 129 patterns of adaptive pleiotropy and discovered that they harbor multiple additional mutations.
 130 This suggests that these populations have not yet reached physiological constraints but rather
 131 that adaptive walks may be constrained by genetic modules which prevent adaptive mutations
 132 from improving multiple performances in a single step.
 133

134 This shows that early adaptation, here represented by the first-step in our evolution experiment,
 135 can engage signaling pathways that allow for rapid, large step pleiotropic adaptation but later
 136 adaptation is more likely to be modular, as expected by theory. We thus expect that longer term
 137 evolution will indeed progress through smaller, and ultimately more modular, adaptive
 138 mutations.



139
 140 **Figure 1. Theoretical illustration: Pleiotropy may be a generic feature of adaptation or specific to**
 141 **the first-step of evolution. (A)** First-step adaptive mutations (each mutation depicted as a dot) in
 142 evolution often exhibit patterns of pleiotropic adaptation - improving performance in multiple traits
 143 simultaneously (falling into the gray square). Gray curved line represents the limits of combinations of
 144 performances reached by the first-step of evolution. **(B)** If pleiotropic adaptation is common, then second-
 145 step adaptive mutations (depicted in red) would continue to improve multiple performances at once.
 146 Longer adaptive walks would also continue to show these patterns (orange arrows). **(C)** If pleiotropic
 147 adaptation is rare and largely constrained to the first adaptive step, then second-step adaptive mutations
 148 might show a shift in their improvement, instead primarily improving one performance or the other (light
 149 red circles). In this scenario, longer term adaptive walks may continue to specialize in one performance or
 150 the other (depicted by blue and magenta arrows), or instead continue to collectively improve both
 151 performances, albeit in a stepwise manner (orange arrows).

152 **RESULTS**

153

154 **Isolating second-step adaptive clones and measuring performance in growth phases**

155

156 When yeast are grown in an environment under glucose-limitation in batch culture, they
157 experience several growth phases (Figure 2A). First, the yeast experience lag phase, where
158 they acclimate to the environment and allocate cellular resources to consuming glucose. Then,
159 the yeast ferment the glucose, converting it to ethanol. Once the glucose is consumed, the
160 yeast then undergo the diauxic shift and respire on the ethanol they produced during
161 fermentation. Finally, once the supply of ethanol has been depleted, the yeast experience
162 stationary phase, where they allocate resources to surviving without a carbon source. These
163 growth phases are typically thought of as independent processes, with distinct transcriptional,
164 proteomic, and metabolomic profiles that characterize and drive yeast physiology (DeRisi, Iyer,
165 and Brown 1997; Schlossarek et al. 2022; Zampar et al. 2013; Murphy et al. 2015).

166

167 Previously, a population of barcoded yeast was evolved in a 2-Day transfer environment under
168 glucose limitation, where they experienced lag, fermentation, and respiration but not stationary
169 phases before being transferred to fresh medium (Levy et al. 2015; Venkataram et al. 2016).
170 Adaptive mutations isolated from this experiment gained substantial fitness benefits, primarily by
171 constitutively activating one of two glucose-sensing pathways: Ras/PKA and TOR/Sch9
172 (Venkataram et al. 2016). Additionally, 85% of these mutants improved performance in both
173 fermentation and respiration phases, despite the supposed independence of these growth
174 phases. Interestingly, with additional evolution experiments designed to maximize individual
175 performances, Li et al (2019) were able to find evidence of constraints on the first step of
176 evolution such that no single mutation is able to simultaneously maximize both fermentation and
177 respiration performances to the largest extreme of each performance observed individually.

178

179 To understand whether pleiotropic adaptation is common or if instead first-step mutations
180 represent rare solutions that improve both traits under selection, we carried out second-step
181 evolution experiments in the same 2-Day transfer environment, isolated adaptive mutants,
182 identified causative mutations underlying adaptation, and characterized the mutations' effects
183 on performance in the environment's growth phases. Aggeli et al. (Aggeli, Li, and Sherlock
184 2021) previously performed second-step evolution experiments using barcoded populations that
185 carried one of three mutations identified in the first step of evolution: a gain-of-function mutation
186 in *CYR1*, a loss-of-function mutation in *GPB2*, and a gain-of-function mutation in *TOR1*. Here,
187 we used additional barcoded populations derived from two distinct mutations in *IRA1*: one
188 missense mutation and one nonsense mutation (see Methods). We then evolved 2 replicates of
189 each barcoded population in the 2-Day transfer condition, labeled here "Evo2D", for 22 transfers
190 (~176 generations) and isolated adaptive clones (Figure 2B,C). As we were also interested in
191 how the number of traits under selection alters the extent of pleiotropic adaptation, we also
192 evolved the same barcoded populations in a 3-Day transfer condition, herein termed "Evo3D",
193 where populations experienced an additional 12 hours of respiration and 12 hours of stationary

194 phase, and isolated adaptive clones from this additional set of evolution experiments (Figure
195 2A-C; see Methods).
196
197 To assess the extent to which physiological and genetic constraints affect the second-step of
198 adaptation, we quantified each mutant's performance in fermentation, respiration, and stationary
199 growth phases using pooled barcoded fitness assays, as developed previously (Figure 2B;
200 (Venkataram et al. 2016; Y. Li et al. 2018; Y. Li, Petrov, and Sherlock 2019; Kinsler, Geiler-
201 Samerotte, and Petrov 2020; Kinsler et al. 2023). Briefly, we pooled all isolated second-step
202 mutants together with the barcoded mutants from the first step of evolution. We then mixed this
203 pool of barcoded yeast with a set of barcoded neutral lineages and the ancestral strain, such
204 that the barcoded pool started at either 2% or 5% frequency in the population and the neutral
205 barcoded lineages collectively represented 2% of the population (see Methods). We then
206 measured the fitness of each mutant by serially transferring $\sim 5 \times 10^7$ cells for five cycles in 1-,
207 2-, 3-, and 5-Day transfer intervals. At each transfer, we froze down the remaining cells,
208 extracted their DNA, amplified the barcode region with PCR, and then sequenced the barcode
209 region. We then calculated each mutant's fitness relative to the ancestor by comparing each
210 mutant's frequency change with the pool of neutral lineages (Figure 2B, see Methods).
211

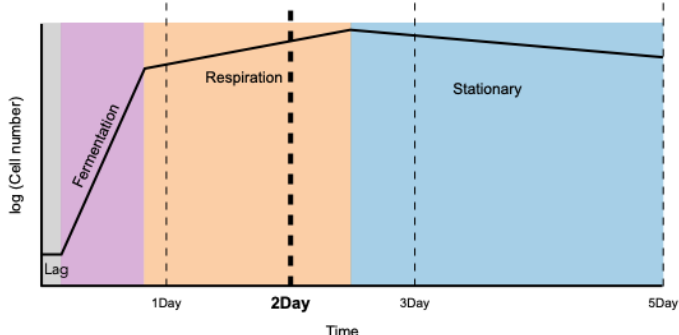
212 During the analysis of fitness measurement data, we observed that the detected fitness effects
213 of each mutant varied systematically over the course of serial transfers during the fitness
214 measurement of the isolated adaptive clones. Specifically, in the 2-Day transfer condition, many
215 adaptive mutants showed very high fitness when the ancestral strain was at or above 80% of
216 the population but showed much lower fitness at later time intervals when the pool of adaptive
217 lineages dominated the population. We note that this effect is not due to change in population
218 mean fitness, as this is already accounted for in these fitness values. While intriguing, we
219 avoided these frequency dependent fitness effects in our data by using only early timepoints,
220 where the ancestor dominated the population, as these reflect the fitness in the environment set
221 by the ancestor and where the fitness of mutants isolated from the original evolution experiment
222 matched their fitness measurements in previous experiments (Figure S1).
223

224 **Second-step adaptive mutations provide substantial yet smaller fitness benefits than** 225 **first-step mutations**

226
227 We sequenced the barcodes in these populations to monitor the dynamics of evolution and to
228 quantify the distribution of fitness effects. Using the approach implemented in software FitMut1
229 (Levy et al. 2015; F. Li, Tarkington, and Sherlock 2023), we quantified the distribution of fitness
230 effects for these populations and the original evolution experiment. Because auto-diploidization
231 is a common mode of adaptation in evolution experiments with haploid yeast, we also used a
232 benomyl assay to determine the ploidy of the isolated adaptive clones (Figure 2C). We then
233 categorized mutants according to their ploidy status and fitness across pooled fitness
234 measurement experiments as neutral haploids, pure diploids, adaptive haploids, or high-fitness
235 diploids (diploids that have additional beneficial mutations, see Methods).

236
237 We found that the rate of beneficial mutations is reduced in the second-step of evolution in the
238 2-Day environment, with adaptive mutations that provide fitness benefits of 1.0 or greater (per
239 cycle) becoming much rarer (Figure 2D). This is consistent with the patterns of diminishing
240 returns epistasis commonly observed in microbial evolution experiments (Wiser, Ribeck, and
241 Lenski 2013; Johnson et al. 2021; Aggeli, Li, and Sherlock 2021; Good and Desai 2015;
242 Wünsche et al. 2017; Chou et al. 2011; Kryazhimskiy et al. 2014). While we see this general
243 decrease in the magnitude of the fitness benefit of adaptive mutations, we nonetheless find that
244 many second-step adaptive mutations still have substantial fitness gains in the 2-Day transfer
245 evolution condition. Across all isolated second-step adaptive mutants (excluding auto-diploids
246 and neutral haploids), the average fitness benefit provided is 82% per cycle relative to the
247 parental strain. This is similar across mutants isolated from both 2- and 3-Day evolution
248 experiments (Figure 2E,F). We also sampled rare mutants with fitness advantages as high as or
249 even higher than the most extreme fitnesses observed in the first step of evolution. For
250 example, two mutants isolated from the Evo3D *IRA1-missense* evolution experiments provide a
251 benefit of ~200% above the parental *IRA1-missense* strain, which corresponds to a ~350%
252 fitness advantage per 2-Day cycle over the original ancestor strain (Figure 2E,F). As will be
253 discussed later, these extremely fit mutants represent rare and complex mutations, sometimes
254 consisting of up to four distinct adaptive mutations.
255
256 We also calculated the relative fitness improvement provided by auto-diploidization alone by
257 comparing the fitness of the pure diploid population to the neutral haploids for each parental
258 strain. Consistent with the pattern of diminishing epistasis observed from the evolution
259 trajectories, we find that the fitness benefit of auto-diploidization has decreased in the second
260 step of evolution from 95% per cycle in the first-step of evolution to 63% on average across all
261 second-step auto-diploids (Figure 2F). However, this number varied by parental strain, with
262 *TOR1* auto-diploids providing the largest fitness benefit of 81% per cycle and auto-diploids of
263 Ras/PKA parental strains providing fitness benefits of 55%, 48%, and 52% per cycle to *CYR1*,
264 *GPB2*, and *IRA1-missense*, respectively (Figure 2F). Surprisingly, we did not isolate any auto-
265 diploids from the *IRA1-nonsense* evolution experiments. We suspect this could be due to
266 differences in the fitness benefit provided by auto-diploidization to *IRA1-nonsense* strains
267 compared to other beneficial mutations in the same evolving population or reduced auto-
268 diploidization rate in this genetic background.

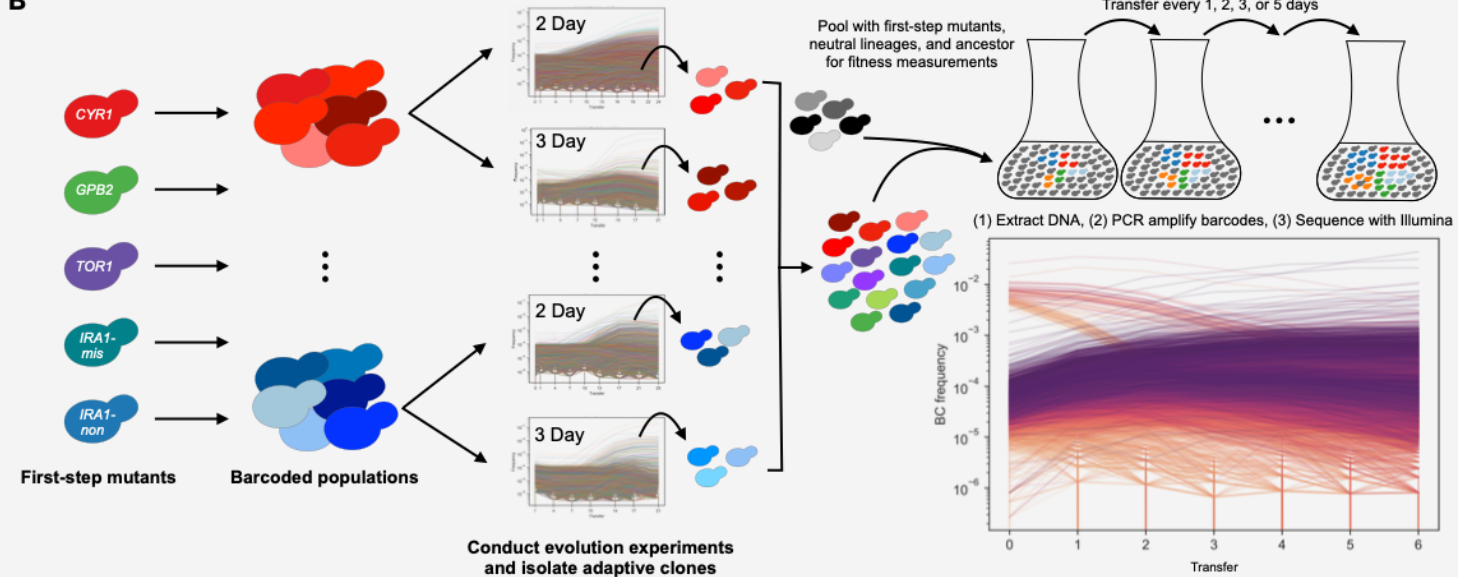
A



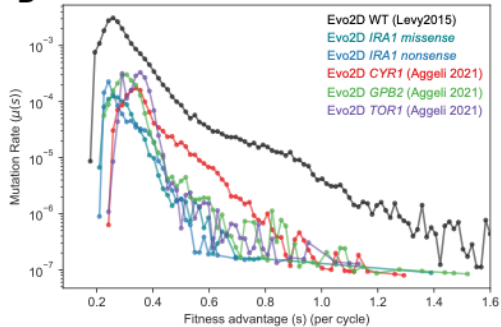
C

	Parental Genotype	First-step mutation	Evolution Condition	Number of adaptive mutants	Number of diploids	Publication
First Step	WT	-	2Day	121	194	Venkataram et al. 2016
Second Step	<i>CYR1</i>	<i>cyr1 S917Y</i>	2Day	68	224	Aggeli et al. 2021
			3Day	20	8	This study
Second Step	<i>GPB2</i>	<i>gpb2 Y282*</i>	2Day	17	228	Aggeli et al. 2021
			3Day	12	20	This study
Second Step	<i>TOR1</i>	<i>tor1 F1712L</i>	2Day	57	317	Aggeli et al. 2021
			3Day	2	-	This study
Second Step	<i>IRA1 missense</i>	<i>ira1 A1211V</i>	2Day	90	16	This study
			3Day	28	3	This study
Second Step	<i>IRA1 nonsense</i>	<i>ira1 L1401*</i>	2Day	95	-	This study
			3Day	135	-	This study

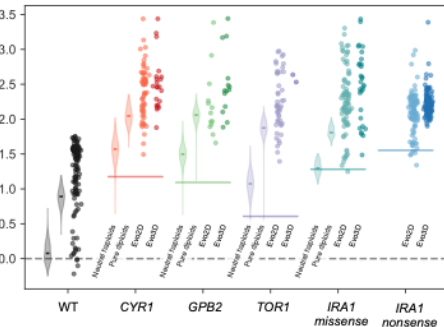
B



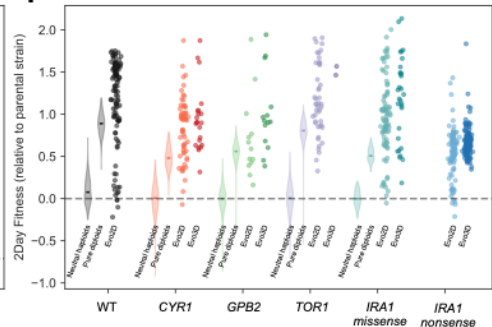
D



E



F



269 **Figure 2. Summary of experiments and fitness effects of isolated adaptive mutants. (A)** A
270 schematic of yeast growth phases under the nutrient conditions used in this study. The yeast experience
271 4 hours of lag phase, 16 hours of fermentation and 4 hours of respiration phase in the first 24 hours of
272 growth. **(B)** Schematic of barcoded evolution experiments and fitness measurement experiments. **(C)**
273 Table of mutants used in this study, including ploidy, and publication source. **(D)** Probability density of
274 mutational fitness coefficients. The black line refers to first-step mutants from Levy et al 2015. Colored
275 lines depict the inferred density of fitness effects of mutations from second-step evolution experiments in
276 the 2Day transfer environment (Evo2D). **(E)** Fitness effects per cycle in 2-Day transfer of all mutants,
277 relative to WT ancestor. First violin plot for each parental strain shows neutral haploids. Second shows
278 pure diploids. Third column is all other 2-Day adaptive mutants, including adaptive haploids and high-
279 fitness diploids. Fourth column is all other 3-Day adaptive mutants. **(F)** As in (E), but relative to parental
280 strain.

281 **Second-step adaptive clones demonstrate a shift from pleiotropic to modular adaptation**

282
283 Next, to determine whether the pattern of pleiotropic adaptation observed over the first-step of
284 evolution is maintained in the second step, we compared changes in performance for each
285 mutant to its parental strain. To calculate each mutant's performance in fermentation,
286 respiration, and stationary phases, we leveraged differences in each mutant's fitness in
287 experiments of different transfer lengths, which was previously shown to be a good proxy for the
288 direct performance in each growth phase (Y. Li et al. 2018; Y. Li, Petrov, and Sherlock 2019). In
289 particular, a mutant's respiration performance per hour was calculated as the difference
290 between its 2-Day fitness and 1-Day fitness, divided by the 24 hours in respiration phase
291 experienced over the second day (Figure 3A). We then used this respiration performance to
292 extrapolate the mutant's relative fitness at 20 hours, the time at which the population undergoes
293 the diauxic shift from fermentation metabolism to respiration metabolism, with which we can
294 calculate its fermentation performance per hour (Figure 3A). Finally, we calculated a mutant's
295 stationary performance by taking the difference between 5- and 3-Day fitness and dividing it by
296 the 48 hours of stationary phase experienced over these two days (Figure 3A). Importantly, the
297 growth phase performances calculated here reflect compound measurements of several
298 parameters important to fitness during and between growth phases, including energy
299 metabolism, sensing of changing nutrient gradients, and survival.

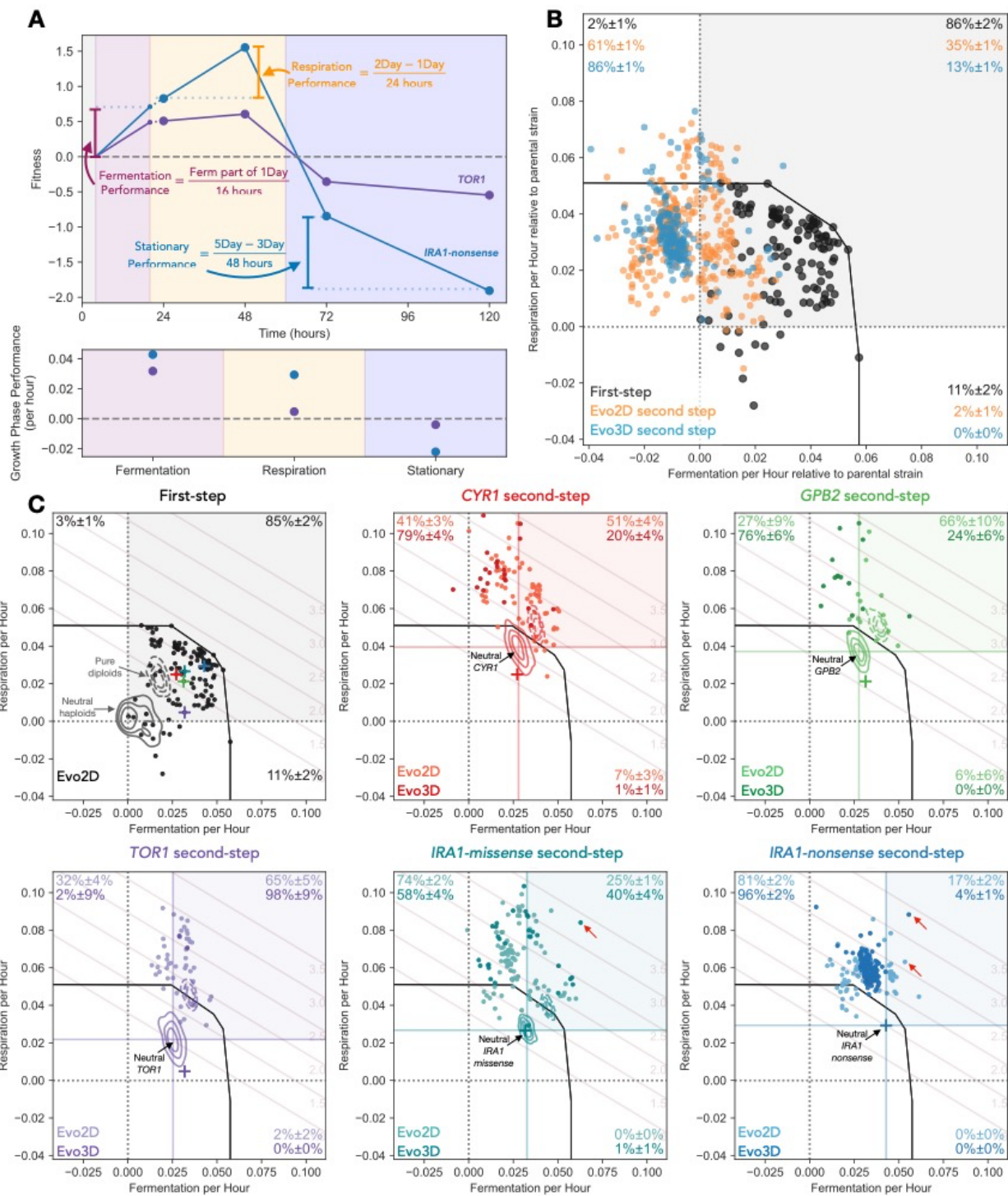
300
301 We found that while 85% ($\pm 3\%$) of isolated first-step adaptive mutants improved performance in
302 both fermentation and respiration phases (black points within gray square in Figure 3B), only
303 35% ($\pm 1\%$) ($p < 0.001$, re-sampling test) of isolated second step adaptive haploids evolved in the
304 same 2-Day transfer environment improved performance over their first-step parental strain in
305 both phases (light orange points within gray square in Figure 3B). Second-step mutants that
306 were isolated from Evo3D, which encompasses the growth phases of Evo2D, show an even
307 stronger shift from adaptive pleiotropy than the second-step mutants from the Evo2D, with only
308 13% ($\pm 1\%$) of these mutants improving performances in both fermentation and respiration
309 (darker colored points labeled "Evo3D" in Figure 3B, C). This shift is also seen for each parental
310 strain individually (Figure 3C), with Evo2D second-step mutants isolated from each first-step
311 parental strain showing a reduction in the number of mutations that improve performance in
312 both fermentation and respiration, albeit with some variability in magnitude. For example, only
313 25% ($\pm 2\%$) and 17% ($\pm 2\%$) of second-step Evo2D mutants from *IRA1-missense* and *IRA1-*
314 *nonsense* parental strains, respectively, improved both fermentation and respiration
315 performances (Figure 3C). At the same time 51% ($\pm 4\%$), 65% ($\pm 10\%$), and 65% ($\pm 5\%$) of
316 second-step Evo2D mutations improve both fermentation and respiration performances from
317 *CYR1*, *GPB2*, and *TOR1*. Thus while the second step adaptive mutations are still capable of
318 improving fermentation and respiration performances at the same time, the probability of
319 mutations being pleiotropically adaptive is lower.

320
321 In addition to a reduction in the number of second-step mutations that improve performance in
322 both fermentation and respiration phases, we noticed that second-step mutants were much

more likely to improve respiration performance than fermentation performance. Across all second-step Evo2D mutants, 98% ($\pm 1\%$) improved respiration performance. 61% ($\pm 1\%$) of these mutants improved respiration at the cost to fermentation performance (Figure 3B). This effect is even stronger for Evo3D mutants, where 86% ($\pm 1\%$) improve respiration at a cost to fermentation performance (Figure 3B). This trend holds across most parental strains, with the strongest pattern seen for mutants evolved from the *IRA1-nonsense* parental strain, where 81% ($\pm 2\%$) of Evo2D mutants and 96% ($\pm 2\%$) of Evo3D mutants improved respiration performance at the cost of fermentation performance. Note that while many of these mutants reduce fermentation performance from the initial first-step parental strains, only a small number of mutants have fermentation performances worse than the original ancestor strain (Figure 3C, vertical black dashed line in each subplot).

At the same time, improving performance in only the fermentation phase is rare. Only 2% of second-step Evo2D mutants and no isolated second-step Evo3D mutants improve fermentation alone, despite the fact that an equivalent improvement in fermentation performance would result in similarly high fitnesses for those mutants in the 2-Day condition these populations were evolved in (see fitness isoclines in Figure 3C).

Despite these general patterns revealing a shift from pleiotropic to modular adaptation, there are several examples of very strongly adaptive clones which improve both performances. For example, one clone isolated from the *IRA1-missense* population has a fitness advantage of 340% per cycle relative to the initial ancestor (or 210% relative to the *IRA1-missense* parental strain). This mutant does improve performance in both fermentation and respiration growth phases, albeit with most of its fitness gain coming from respiration (Figure 3C, *IRA1-missense* panel, labeled with red arrow). We isolated other rare examples of very fit clones that improve both growth phases from other parental strains (Figure 3C, *IRA1-nonsense* panel, labeled with red arrows), suggesting that the yeast have not yet reached functional constraints on the ability to improve both fermentation and respiration performance and that it is still possible to improve both performances beyond the evolutionary constraints observed for the first step of adaptation. As discussed below, some of these very fit clones have acquired third or fourth adaptive steps, allowing them to achieve these high fitnesses.



354 **Figure 3. Second-step adaptive mutants tend to improve respiration performance and not**
355 **fermentation performance.** (A) Performance calculation in each growth phase. Respiration performance

356 (per hour) is calculated as the difference between a mutant's 2-Day and 1-Day fitness, divided by 24

357 hours. To calculate fermentation performance (per hour), we remove four hours of 1-Day fitness that is

358 due to the mutant's respiration benefit. The remaining fitness is then divided by 16 hours of fermentation

359 phase. Stationary phase performance (per hour) is calculated as the difference between 5- and 3-Day

360 fitness divided by 48 hours. Example fitnesses and performances are shown for the *TOR1* and *IRA1-*

361 *nonsense* mutations used as parental strains for the second-step of evolution. (B) Comparison of

362 changes in performances from first- to second-step mutants relative to each parental strain. Note that

363 first-step mutants are shown relative to the initial ancestor (the same as their measured fitness). Second-
364 step mutants are shown relative to the relevant parental strain (i.e. second-step mutants from *IRA1*-
365 missense are shown relative to neutral *IRA1-missense* parental lineages). Percentages in corners
366 indicate estimated fraction of mutants in each quadrant as determined by re-sampling of mutants with
367 fitness measurement error. **(C)** Performance of isolated mutants separated by parental strain. Each
368 mutant's performance in fermentation and respiration growth phases is shown, separated into subfigures
369 by the initial ancestor for each mutant. KDE estimates represent the density of neutral haploids (solid
370 lines) and pure diploids (dashed lines) for each ancestor. Crosses represent the barcoded mutants
371 carrying the first-step mutation from the initial evolution experiment. Black line depicts a convex hull of the
372 most extreme first-step mutants. Fitness isolines show the 2-Day fitness advantage per cycle relative to
373 ancestral strain associated with each location in the performance space.
374

375 **Adaptively modular second-step mutants are more likely to improve performance in
376 stationary phase**

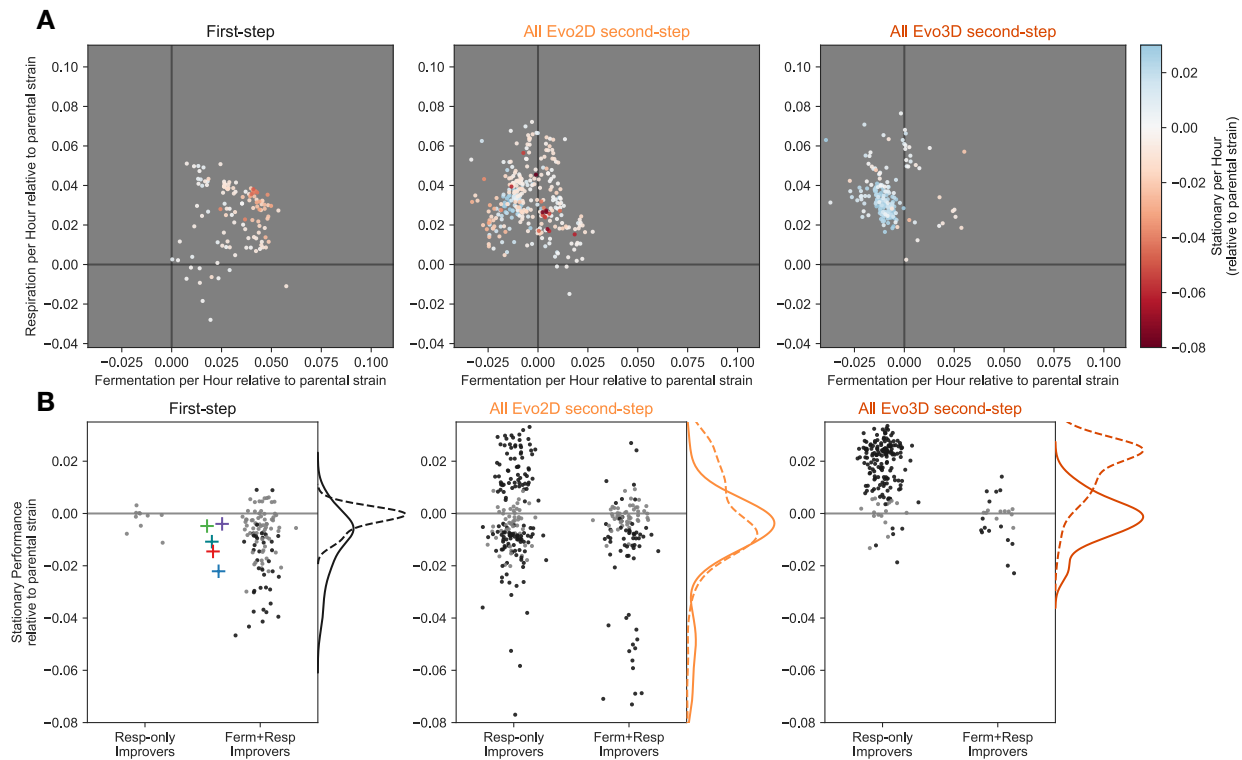
377 We next asked how the shift from adaptive pleiotropy to adaptive modularity of performances
378 under selection affects how these mutants perform in other tasks not under selection in the
379 Evo2D environment. For example, Li et al (2018) (Y. Li et al. 2018) showed that many of the
380 first-step mutations, which tended to improve both fermentation and respiration performances,
381 exhibited costs in stationary phase performance. Does the shift towards adaptive modularity
382 reduce the likelihood or magnitude of costs in other performances, potentially indicating that
383 these mutants are more modular overall? Or do these costs to other performances remain?
384

385 To address these questions, we calculated each mutant's performance in stationary phase
386 (Figure 2A). As previously described (Y. Li et al. 2018), first-step mutants are more likely to
387 incur a cost in stationary phase than to improve it (Figure 4A), with 30% (36/119) of mutants
388 showing such a cost (Figure 4B) and less than 2% (2/119) showing any improvement in
389 stationary performance. The most fit first-step mutants which improve both fermentation and
390 respiration performance to substantial degrees tend to have larger costs in the stationary phase.
391 In particular, the *IRA1*-nonsense mutants, which were the most fit in the first-step, have the
392 strongest costs in stationary phase performance, up to -4% per hour (Figure 4A).
393

394 We find that many Evo2D second-step mutants do pay a cost in stationary phase. In particular,
395 42% of second-step Evo2D adaptive mutants have lower stationary performance than their
396 parental strain. At the same time, these costs to stationary performance tend to be somewhat
397 minor, exhibiting costs of less than -2% per hour for second-step mutants derived from *CYR1*,
398 *GPB2*, *TOR1*, or *IRA1*-missense parental strains (Figure 4B). Note that this was not the case for
399 the second-step mutants isolated from *IRA1*-nonsense populations, which exhibited the
400 strongest costs to stationary phase in the first-step of evolution. These second-step mutants had
401 further costs to stationary performance as extreme as -10% per hour (see supplemental figures
402 S3 and S4).
403

405 However, in contrast to the first-step of evolution where stationary performance was rarely
406 improved, 25% (77/306) of second-step Evo2D mutants show an increase in stationary
407 performance (Figure 4A). We further stratified the second-step mutants based on their
408 combined fermentation and respiration performances. Specifically, we asked whether mutants
409 that only improve respiration performance showed behavior in stationary phase that was distinct
410 from those that improved both fermentation and respiration performance. We find that second-
411 step Evo2D mutants that only improved respiration performance had varied effects on stationary
412 performance, with 36% (70/197) showing increased stationary performance and 39% (76/197)
413 showing a cost to stationary performance. By contrast, second-step Evo2D mutants that
414 improved both fermentation and respiration performances were much less likely to improve
415 stationary performance, with only 6% (7/109; $p < 1e-8$ compared to by respiration-only improvers
416 by Fisher's exact test) of these mutants showing stationary improvement and 49% (53/109)
417 imposing a cost on yeast's ability to survive stationary phase.
418

419 Thus, it appears that mutations that are capable of improving both fermentation and respiration
420 at the same time are more likely to incur costs in stationary phase. This inherent relationship
421 may explain the reduction in Evo3D mutants that improve both fermentation and respiration
422 performances (Figure 3B, 4A), as stationary phase is additionally under selection in this
423 condition. Indeed, 79% (160/202; $p < 1e-8$ compared to Evo2D by Fisher's exact test) of Evo3D
424 mutants show an improvement in stationary phase, 97% (155/160) of which do not improve
425 fermentation. While 7% (15/202) of Evo3D mutants do exhibit a cost in stationary phase, these
426 costs are relatively minor and are primarily found in mutants with combined fermentation and
427 respiration performances that compensate for these costs to stationary performance (Figure 4A
428 and B). These data indicate that the shift from mutants that improve both fermentation and
429 respiration performances to those that primarily improve respiration performance is
430 accompanied by a change in stationary phase performance. This pattern is true even when the
431 other performance (stationary phase) is not under selection, as is in the case of Evo2D,
432 suggesting that the pleiotropic "side effects" - that is phenotypic effects of mutations that are not
433 primarily under selection (Kinsler, Geiler-Samerotte, and Petrov 2020) - of these second-step
434 mutants may differ more generally from those of the first-step mutants.



435
436
437
438
439
440
441
442
443
444
445
446
447

Figure 4. Mutations that improve respiration performance only exhibit less extreme costs in stationary phase compared to those that improve fermentation and respiration performances. (A) Each panel depicts mutant performance relative to their parental strain, colored by the relative stationary phase performance of the parental strain (see color bar). The first panel shows all first-step mutants. The second and third panels depict second-step mutants isolated from Evo2D and Evo3D conditions, respectively. (B) Each panel shows the stationary performance relative to the mutants' respective parental strains. Mutants are split according to the effect on fermentation and respiration performances. Those which improve both fermentation and respiration are categorized as "Ferm+Resp Improvers" and all other mutants are categorized as "Resp-only improvers". Black points represent those with measurement error that does not overlap 0. Gray points have measurement error that show no significant change in stationary performance relative to the parental strain. Panels are organized as in (A). Kernel density estimates show the relative density for respiration-only improvers (dashed line) and fermentation and respiration-improving mutants (solid line).

448

449 Changes in selection pressure and physiological limitations do not explain the shift 450 towards modular adaptation

451

452 Thus far, we have shown that there is a general shift in the effect that adaptive mutations have
453 on performance in growth phases over the course of a two-step adaptive walk. In particular, we
454 find that while first-step mutations exhibit adaptive pleiotropy, improving both fermentation and
455 respiration performances, second-step mutations isolated from the same Evo2D environment
456 tend to be adaptively modular, improving only respiration performance and often at the cost to
457 fermentation performance. What could be driving this shift? There are three primary possibilities
458 for this observation. One possibility is that, while care was taken to ensure the evolution
459 condition was as consistent as possible to the first step of evolution, the selection pressure in

460 the second-step evolution experiments was shifted to favor respiration performance more than
461 fermentation performance. A second possibility is that the populations have reached
462 physiological limits on the yeast's ability to ferment glucose, such that there is more room to
463 improve respiration performance. Finally, it could be that genetic and signaling pathways are
464 wired such that there are only a limited number of mutational targets available to further improve
465 both fermentation and respiration performances in the second-step of evolution.

466

467 The first possible explanation for the shift towards modular adaptation is that the second-step of
468 evolution was accompanied by a change in the relative contribution of fermentation and
469 respiration growth phases to fitness in the 2-Day transfer condition. While we took care to
470 ensure that the population sizes, transfer times, media conditions, and other details were
471 identical to the conditions used in the first-step evolution experiment, it could be possible that
472 differences remain. For example, the identity of the strain comprising the majority of the
473 population in second-step evolution experiments may have shifted the selection pressures to
474 increase the importance of respiration performance compared to the first step of evolution. To
475 test whether there was such a shift, we compared the fitness effects of mutations in the
476 evolution experiment itself with our fitness measurement experiments, which more closely mimic
477 the first-step evolution experiments because the ancestral strain comprises the majority of the
478 population. Specifically, we calculated the partial correlation between respiration performance
479 and fitness during the evolution experiment, accounting for the fitness inferred from our fitness
480 measurement experiments. If respiration performance contributes more to evolution fitness than
481 expected from our fitness measurement experiments, we would expect a positive partial
482 correlation after this adjustment. However, this is not the case ($r=-0.02$, $p=0.74$), indicating that
483 the shift from pleiotropic to modular adaptation is not due to a change in selection pressure (see
484 Methods, Differences in selection pressure do not drive shift towards modular adaptation).

485

486 The second possible explanation for the shift towards modular adaptation is that the yeast have
487 reached physiological limits on the ability to improve fermentation performance. To test whether
488 yeast have reached the upper limits of fermentation performance, we performed additional
489 evolution experiments in a 1-Day transfer environment, which primarily selects for fermentation
490 performance. From these experiments, we isolated at least one second-step mutation from the
491 *IRA1*-nonsense population that improved fermentation performance above the highest
492 fermentation performances achieved by first- or second-step mutations evolved in the 2-Day
493 and 3-Day environments (see Fig S2). This suggests that while a fermentation performance
494 maximum has not yet been reached, the pre-existing wiring of genetic and signaling pathways
495 may be such that it is much easier to find mutations that improve respiration performance at the
496 cost of fermentation performance than it is to find mutations that improve both fermentation and
497 respiration performances or even fermentation performance at the cost to respiration
498 performance.

499 **Second step adaptive mutations reveal a shift from mutational targets in general nutrient-**
500 **sensing pathways to specific processes involved in mitochondrial function**

501
502 To better understand these patterns of pleiotropy and to identify the genetic basis of adaptation
503 in these environments, we performed whole-genome sequencing on 324 adaptive mutants and
504 called variants (see Methods). To identify the likely adaptive mutations, we compared the genes
505 across all isolated mutants from all evolution experiments and labeled genes that were hit more
506 than three times across all mutants as putatively causal. After identifying pathways that were
507 recurrently targeted, we further identified genes belonging to the same pathways and called
508 these as putatively causal as well.

509
510 From this whole-genome sequencing, we found some adaptive targets in nutrient-sensing
511 pathways that were previously identified in the first-step of evolution. The first-step of adaptation
512 typically involved mutations in one of two signaling pathways responsible for sensing glucose
513 and instructing the cells to grow: the Ras/PKA and TOR/Sch9 pathway (Venkataram et al.
514 2016), Table 1). Most of these mutations resulted in loss of function in negative regulators of the
515 pathway or modification of function in positive regulators, ultimately driving constitutive
516 activation of these pathways (Venkataram et al. 2016). In an analysis of the second-step of
517 evolution for *TOR1*, *CYR1*, and *GPB2* mutants in the 2-Day environment, Aggeli et al (2021)
518 identified Ras/PKA pathway mutations as an adaptive route for *TOR1* mutants and TOR/Sch9
519 mutants as an adaptive route for *CYR1* and *GPB2* mutants. The additional sampling we've
520 conducted here, including sequencing mutants isolated from the two *IRA1* populations under
521 Evo2D and Evo3D, further confirm that TOR/Sch9 pathway mutations are commonly observed
522 in the background of Ras/PKA mutants. In particular, we find that mutations in the gene *KSP1*, a
523 PKA-activated kinase which inhibits autophagy via TORC1 (Umekawa and Klionsky 2012;
524 Chang and Huh 2018), are common across all of the Ras/PKA parental strains (Table 1). These
525 mutations were most commonly isolated from *IRA1*-nonsense populations, where 42% (32/77)
526 of Evo2D mutants and 91% (30/33) of Evo3D mutants harbored a *KSP1* mutant. Unlike the
527 TOR/Sch9 pathway mutants observed in the first-step of evolution, which putatively result in
528 increased TORC1 activity, increased cell growth, and decreased autophagy (Wilson and Roach
529 2002; Venkataram et al. 2016), many of the observed second-step *KSP1* mutations are loss-of-
530 function . This indicates that these mutations may be acting in the opposite direction of first-step
531 mutations in this pathway, potentially allowing for the up-regulation of TOR despite (or in
532 compensation of) increased activation of PKA associated with the Ras/PKA mutants.

533
534 Beyond mutations in nutrient-sensing signaling pathways commonly being observed in the first-
535 step of adaptation, our sampling reveals a shift towards mutational targets related to
536 mitochondrial function and respiration, which likely affect the respiration performance of mutants
537 measured in our study (Table 1). In particular, we find that 36% (22/64) of adaptive mutants
538 isolated from *IRA1*-missense populations in the 2-Day evolution condition acquire mutations in
539 or near genes involved in the TCA cycle (*CIT1*, *KGD1*, *MDH1*, *MAE1*, *ALD5*). Interestingly, all of
540 these mutations are either missense or putatively regulatory mutations in enzymes directly

541 responsible for respiration, suggesting they may modify the function or expression of these
542 enzymes, potentially changing respiratory flux (Suissa, Suda, and Schatz 1984; Kurita and
543 Nishida 1999; Navarro-Aviño et al. 1999; Repetto and Tzagoloff 1989; Ait-EI-Mkadem et al.
544 2017; Reinders et al. 2007; McAlister-Henn and Thompson 1987; Boles Eckhard, de Jong-
545 Gubbels Patricia, and Pronk Jack T. 1998). In addition, we identified mutations in several genes
546 related to the regulation of respiration and mitochondrial function, with 25% (16/64) of isolated
547 2-Day *IRA1*-missense mutants identified as carrying a mutation in the RTG pathway, which is
548 responsible for the regulation of genes important for respiration. In particular, we observe
549 putative loss-of-function mutations in *MKS1*, a negative regulator of the RTG pathway, and
550 missense mutations in *RTG2*, a positive regulator of the pathway (Liu et al. 2003; Liao and
551 Butow 1993; Komeili et al. 2000; T. Sekito, Thornton, and Butow 2000; Takayuki Sekito et al.
552 2002). This suggests that these mutations may be up-regulating the RTG pathway and the
553 genes it regulates, indirectly increasing metabolic flux through the TCA cycle. Moreover, 19%
554 (12/64) of these mutants carry a mutation in other genes related to the regulation of
555 mitochondrial biogenesis (*PUF3*, *PAB1*, *PAN1*, *PAN2*, *AIM17*), many of which are related to
556 post-transcriptional modification of mRNA molecules related to mitochondrial function or
557 respiration (Chaithanya and Sinha 2023; C.-D. Lee and Tu 2015; Lapointe et al. 2018).

558
559 These patterns are also observed in other populations harboring different first-step mutants. In
560 particular, while our sampling for *IRA1-nonsense* and *IRA1-missense* populations allowed us to
561 detect the largest number of mutational targets, mutations in genes involved in the TCA cycle,
562 RTG pathway, and mitochondrial biogenesis were found in populations from nearly all first-step
563 mutations, with a few exceptions. These exceptions, for example the absence of HOG-pathway
564 mutations from *IRA1-missense* and *IRA1-nonsense* backgrounds, is suggestive of historical
565 contingency, where the identity of further mutations is dependent on mutations acquired earlier
566 in evolution (Blount, Borland, and Lenski 2008; Harms and Thornton 2014; Park, Metzger, and
567 Thornton 2022; Bakerlee et al. 2021). While some of these genes were detected in previous
568 work (Aggeli, Li, and Sherlock 2021), additional sampling from new evolution experiments in the
569 3-Day condition and additional parental strains (*IRA1-missense* and *IRA1-nonsense*) allowed us
570 to more confidently identify recurrently mutated genes and to group the observed sets of
571 mutations and genes into functional categories and pathways.

572
573 **Mutations isolated from the 3-Day evolution experiment are a subset of 2-Day adaptive**
574 **mutants**
575

576 We next examined whether there was a difference in the mutational targets isolated from 2- and
577 3-Day evolution experiments, given that we observed that Evo2D mutants were more likely to
578 improve both fermentation and respiration performances than Evo3D mutants (Figure 3), and
579 Evo3D mutants were more likely to improve stationary performance than Evo2D (Figure 4). In
580 particular, we wondered whether the addition of stationary phase as a selective pressure
581 allowed for new mutational targets to be adaptive because of their effect on stationary phase, or

582 if instead, the addition of stationary phase restricted the Evo3D mutational targets to a subset of
583 the Evo2D mutations that were not costly to stationary performance.

584

585 By comparing the sets of mutated genes for well-sampled parental strains *IRA1-missense* and
586 *IRA1-nonsense*, we saw that all genes mutated in the 3-Day evolution experiments were also
587 identified in the 2-Day evolution experiments (see Table 1). In particular, *PUF3*, *PAB1*, and
588 *MTH1* mutants are entirely absent as single mutations from the 3-Day *IRA1-nonsense*
589 experiments, shifting the molecular targets to essentially just those in *KSP1*. Similarly, RTG and
590 TCA cycle mutants are reduced in frequency or absent from the 3-Day *IRA1-missense*
591 experiments, respectively. As expected, these mutations that are reduced in frequency show
592 costs in stationary performance and thus have reduced fitness in the 3-Day transfer
593 environment (Figs S7 and S8).

594

	WT	<i>TOR1</i>		<i>GPB2</i>		<i>CYR1</i>		<i>IRA1-missense</i>		<i>IRA1-nonsense</i>		
	Evo2D	Evo2D	Evo3D	Evo2D	Evo3D	Evo2D	Evo3D	Evo2D	Evo3D	Evo2D	Evo3D	
Ras/PKA Pathway	<i>IRA1</i> 30/77								1/30*			Loss of function
	<i>IRA2</i> 11/77		1/21									Loss of function
	<i>GPB1</i> 4/77				1/7*							Modification of function
	<i>GPB2</i> 14/77		2/21									Loss of function
	<i>PDE2</i> 11/77											Loss of function
	<i>CYR1</i> 3/77											Modification of function
	<i>GPR1</i>						1/27					Modification of function
	<i>RAS2</i> 1/77		1/21									Modification of function
TOR/Sch9 Pathway	<i>TOR1</i> 1/77											Modification of function
	<i>KOG1</i> 1/77											Modification of function
	<i>SCH9</i>			1/7								Modification of function
	<i>KSP1</i>			1/7	1/8*	1/27	2/14	4/67		32/72	30/33	Loss of function
HOG Pathway	<i>HOG1</i>					1/27						Modification of function
	<i>PBS2</i> 6/21											Modification of function
	<i>SSK2</i> 7/21		1/7	1/8	1/27							Loss of function
	<i>RTG2</i>				1/8	4/27	2/14	9/67	1/30	1/72		Modification of function
RTG Pathway	<i>MKS1</i>					2/27	1/14	7/67	1/30*			Loss of function
	<i>BMH1</i>			1/7*		1/27						Modification of function
	<i>CIT1</i> 1/21					1/27		16/67	1/30			Modification of function
	<i>KGD1</i>					1/27		3/67				Modification of function
TCA cycle	<i>MDH1</i>							4/67				Modification of function
	<i>MAE1</i>							2/67		2/72*		Modification of function
	<i>ALD5</i>						1/14	1/67*			2/33*	Modification of function
	<i>PAB1</i> 1/21				2/8	1/27	4/14	3/67	5/30	12/72		Modification of function
Regulation of Mitochondrial Biogenesis	<i>PAN2</i>							2/67				Modification of function
	<i>PAN3</i> 1/21							1/67				Loss of function
	<i>AIM17</i>				1/8			2/67				Loss of function
	<i>PUF3</i>				1/8	4/27	2/14	7/67	7/30	24/72	1/33*	Loss of function
Other	<i>MKT1</i>		1/7	1/8		1/27	1/14	1/67	9/30			Modification of function
	<i>GSH1</i> 1/21		1/7			5/27		2/67	1/30	1/72*		Modification of function
	<i>ARO80</i>					3/27	1/14	3/67	4/30			Loss of function

595
596 **Table 1. Identified mutations by ancestral genotype and evolution condition.** Boxes with gray text
597 and asterisks indicate genes mutated only in the context of other putatively causal mutants. The column
598 on the far right indicates the putative functional effect of the mutations on the gene. If any stop-gained or
599 frameshift mutations were identified in this gene, it was classified as harboring “loss of function”
600 mutations. If instead, only missense or nearby non-genic mutations were identified, the gene is classified
601 as “modification of function”.

602 **The exhaustion of mutational targets in nutrient-sensing signaling pathways drives the**
603 **shift towards modular adaptation**

604
605 To understand how the shift from pleiotropic to modular adaptation over the two-step adaptive
606 walk is reflected on a molecular basis, we examined how each of these mutations moved the
607 organisms in the performance space. The first step of evolution, which primarily hit mutational
608 targets in the Ras/PKA pathway, shows strong patterns of pleiotropic adaptation, with these
609 mutations improving both fermentation and respiration performances (Figure 5A).

610
611 Of the second-step adaptive haploids, those with mutations in the Ras/PKA pathway (Figure 5B,
612 blue circles), which were isolated primarily from the *TOR1* populations, also display pleiotropic
613 adaptation, improving both fermentation and respiration performance. This suggests that
614 mutations which putatively increase the activity of the Ras/PKA pathway are indeed generally
615 adaptively pleiotropic.

616
617 In addition to Ras/PKA mutations, other haploids with mutations in *ARO80* (Figure 5B, pink
618 circles) and *GSH1* (Figure 5B, gold circles), show recurrent patterns of pleiotropic adaptation
619 across parental strains, notably across *CYR1* and *IRA1*-missense genetic backgrounds (Figures
620 S5 and S6). Mutations in these genes, which are involved in amino acid catabolism (Iraqui et al.
621 1999; K. Lee and Hahn 2013) and glutathione biosynthesis (Kistler, Maier, and Eckardt-Schupp
622 1990), respectively, may be adaptively pleiotropic due to their involvement in processes entirely
623 orthogonal to, or upstream of, both fermentation and respiration.

624
625 Many of the remaining mutational targets improve respiration performance at the cost of
626 fermentation performance. In particular, haploid mutants which harbor mutations in genes
627 involved in the TCA cycle (Figure 5B, green circles), mitochondrial biogenesis (orange, red
628 circles), or the RTG pathway (brown circles) improve respiration performance at the cost to
629 fermentation performance in *CYR1*, *GPB2*, *TOR1*, and *IRA1*-missense backgrounds when
630 present (Figure 5). Notably, haploids that harbor mutations in these genes have similar fitness in
631 the 2-Day transfer environment to mutants with mutations in *ARO80* and *GSH1*, which exhibit
632 adaptive pleiotropy. Despite these similar fitnesses, there is an 8-fold increase in observed
633 adaptively modular genetic targets than those that are adaptively pleiotropic in the *IRA1*-
634 missense 2-Day evolution experiments (41 mutants in TCA and RTG with fitnesses between 2.0
635 and 2.5 compared to 5 in *GSH1* and *ARO80* for *IRA1*-missense).

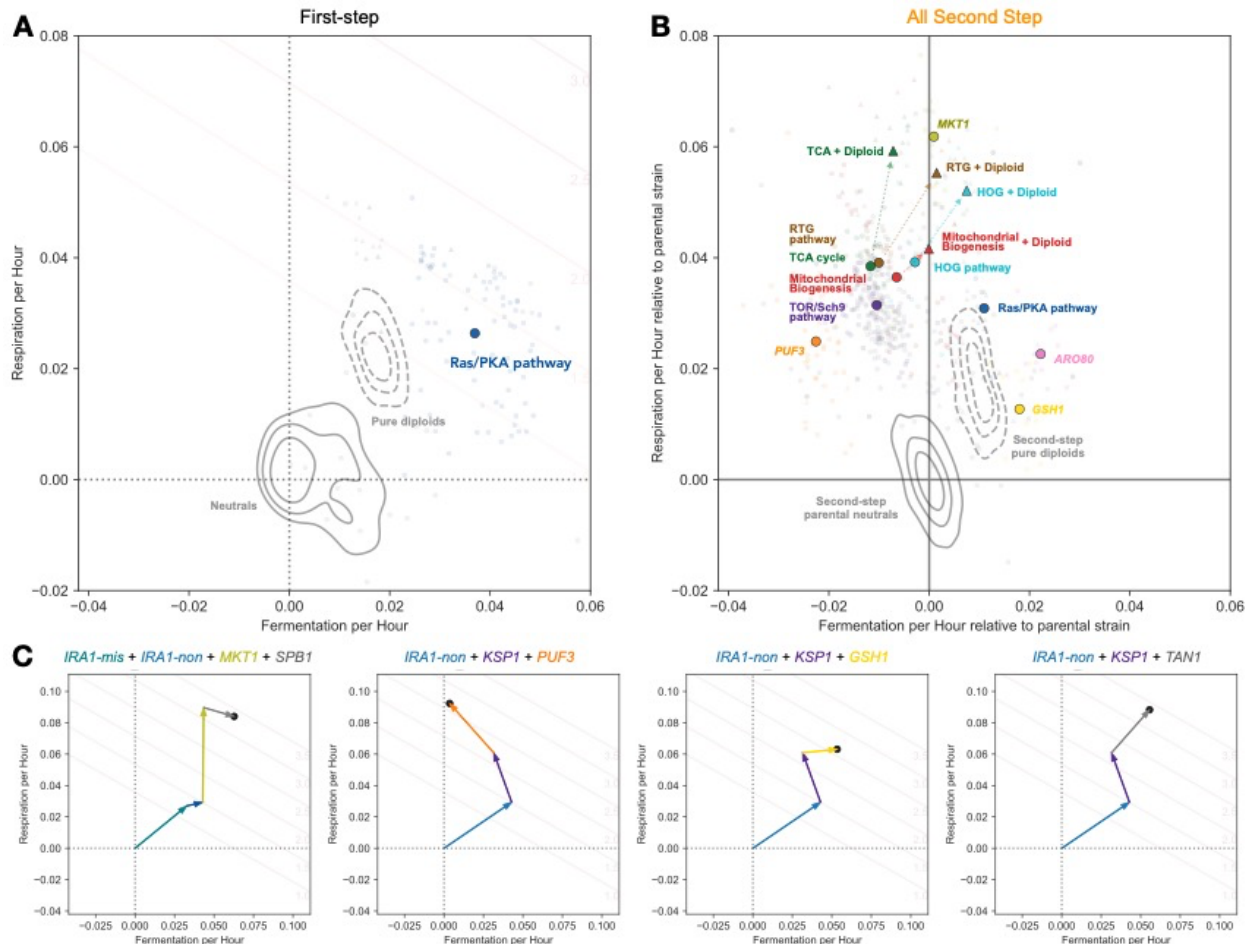
636
637 There are also single point mutations in *MKT1* which achieve very high 2-Day fitness by greatly
638 improving respiration performance and showing little cost to fermentation performance (Figure
639 5B - chartreuse circles). Interestingly, all adaptive mutations in this gene occur at the same
640 nucleotide, changing from 89A to C, G, or T. Thus, while these mutations are driven by only a
641 single mutation, their lower frequency reflects the reduced target size compared to the other
642 haploid mutations which have multiple targets within the gene (e.g., those in RTG pathway, TCA
643 cycle, etc.). The 89A allele is a derived allele in the parental S288C yeast strain used for all of

these experiments and reflects an ancestral reversion in the case of A89G. This A89G reversion has been previously observed in other evolution experiments in glucose limitation and the 89G allele has been shown to stabilize mRNA of mitochondrial genes that are targets of Puf3 (Chaithanya and Sinha 2023; Gupta et al. 2015). Interestingly, 89C and 89T alleles each provide similar fitness benefits as the 89G allele in our experiments despite resulting in distinct amino acids, suggesting that the 89A allele and the resulting aspartic acid may be particularly costly to *MKT1* function.

Beyond adaptive mutations in haploids, auto-diploidization is a common mode of adaptation. In particular, we see that in addition to diploidy being adaptively pleiotropic by itself (pure diploids shown as topographical Kernel Density Estimates in Figure 5), high-fitness diploids that co-occur with other mutations (colored triangles in Figure 5) also show patterns of adaptive pleiotropy, improving both fermentation and respiration performances. This seemingly universal benefit without cost likely explains the high frequency of auto-diploidization observed across genetic backgrounds and environmental conditions in many yeast evolution experiments (Tung et al. 2021; Venkataram et al. 2016; Levy et al. 2015; Hong and Gresham 2014; Fisher et al. 2018). While these high-fitness diploids provide a much larger benefit than haploids that harbor mutations in the same genes, their reduced frequency is likely due to a lower mutation rate, as these mutants needed to acquire both a mutation in an adaptive target and auto-diploidize, together improving respiration to a larger extent and mostly eliminating costs to fermentation performance associated with the mutation. Notably, most of the point mutations are homozygous, indicating they likely occurred before the auto-diploidization event.

In addition to these general trends, we sampled a small number of mutations that have a total of three or four putatively causal mutations since the original ancestor. These mutants provide hints about how adaptation might proceed over longer adaptive walks. In one case, as demonstrated by the *IRA1*-nonsense + *KSP1* + *PUF3* mutant depicted in the second panel of Figure 5C, we observe adaptation as continuing down a route towards specialization in respiration performance. We also observe three examples where the collective effect of the mutations instead drives evolution towards generalism – improving both fermentation and respiration performance – despite being composed of second-, third-, and fourth-step mutations which tend to improve only one performance or the other. For instance, one *IRA1*-missense mutant acquired an *IRA1*-nonsense mutation, an *MKT1* A89G mutation which improves only respiration by itself in this background, and acquired a mutation in *SPB1* (Suppressor of *PAB1*), which is expected to improve only fermentation with a modest cost to respiration, assuming additive mutational effects in the performance space (Figure 5C, first panel). We see similar examples for two *IRA1*-nonsense mutants: one of which acquired both *KSP1* and *GSH1* mutations and the other of which acquired *KSP1* and *TAN1* mutations (Figure 5C, third and fourth panels), where the collective effects of the observed mutations ultimately continue to push the population towards improving both traits. These rare mutants demonstrate that, at least on short evolutionary timescales, navigation of the performance space seems to be more driven by constraints imposed by the genetic wiring of the cell, which influences the relative

686 ease of improving one performance or the other, rather than fundamental or physiological
 687 constraints upon improving the performances themselves.
 688



689
 690 **Figure 5. Adaptive modularity is driven by the accessibility of mutational targets that improve**
 691 **respiration at the cost of fermentation.** (A) Ras/PKA and TOR/Sch9 mutants from the first-step of
 692 adaptation to improve both fermentation and respiration performance. (B) Most common second-step
 693 mutational targets tend to improve respiration at the cost of fermentation (centroids depicted as colored
 694 circles), except for rare Ras/PKA (blue), ARO80 (pink), or GSH1 (yellow) mutants; haploids shown as
 695 circles. Auto-diploids exhibit adaptive pleiotropy (dashed KDE estimate for all parental strains, colored by
 696 first-step mutation). Auto-diploidization is also adaptively pleiotropic on the background of other point
 697 mutations (triangles colored by pathway or gene category). Note that only centroids for each category of
 698 gene with at least 3 observed mutants were included. (C) Triple and quadruple mutants can ultimately
 699 drive adaptation towards adaptive pleiotropy (or adaptive modularity) despite being primarily composed of
 700 adaptively modular mutations. Note that the mutations beyond the first step are depicted in no particular
 701 order in these subpanels.

702 **DISCUSSION**

703

704 In this study, we sought to understand the frequent observation that single adaptive mutations
705 observed in experimental evolution, especially those of large effect, can pleiotropically improve
706 multiple distinct performances at once. This observation is puzzling because theoretical work
707 suggests that as pleiotropy increases, large effect adaptive mutations should become less
708 probable. This expected “cost of complexity” is the reason for why modularity is often seen as
709 the necessary condition and the expected consequence of evolution of complex organisms by
710 natural selection (Orr 2000; Welch and Waxman 2003; Wagner and Zhang 2011; Wagner,
711 Pavlicev, and Cheverud 2007; Wagner and Altenberg 1996; Melo et al. 2016; Hartwell et al.
712 1999).

713

714 We focused on one striking example of pleiotropic adaptation that comes from previous studies
715 of yeast evolving in a glucose-limited environment (Levy et al. 2015) in which 85% of the first-
716 step single adaptive mutations improved performance in both fermentation and respiration
717 growth phases (Fig1A, Fig3B) (Levy et al. 2015; Venkataram et al. 2016; Y. Li et al. 2018),
718 despite these growth phases as being thought to be physiologically distinct.

719

720 Here, we investigated whether adaptation in the same low-glucose environment and 2-Day
721 transfer as the original experiment (Levy et al. 2015) will continue following the path of adaptive
722 pleiotropy (Fig. 1B) or will shift to become more modular (Fig. 1C). We thus further evolved 5
723 different first-step mutants, four in the Ras/PKA pathway (*IRA1-nonsense*, *IRA1-missense*,
724 *CYR1*, and *GPB2*) and one in the Tor/Sch9 pathway (*TOR1*), sampled a large number of
725 adaptive mutants, and evaluated their effects on the fermentation and respiration performances.
726

727 In all five cases, the results were qualitatively similar. First, adaptation proceeded to improve
728 fitness, albeit to a somewhat muted degree. Second, while a number of mutants were adaptively
729 pleiotropic, improving both fermentation and respiration performances, the dominant trend
730 switched towards more modular adaptation. Specifically, nearly all adaptive mutants improved
731 respiration performance sharply and many had no or only weakly positive or even negative
732 effects on the fermentation performance (Fig. 3B). These results support a model of adaptation
733 wherein early adaptation is driven by mutations of large effect that improve multiple
734 performances at once. Then, after these mutations have become exhausted, adaptation may
735 proceed via more modest mutations that improve performances in a stepwise manner (Figure
736 1C).

737

738 One remaining question is how pleiotropic adaptation is possible in the first place. The
739 prevalence of the pleiotropic adaptation in the first step may be due to these mutations being
740 primarily in Ras/PKA pathway genes. We thus hypothesized that the adaptive pleiotropy is a
741 consequence of the way this pathway has evolved to shift rates of metabolism in both
742 fermentation and respiration in a substantial, coordinated, and beneficial fashion (Wilson and
743 Roach 2002). The notion is that even though these metabolic functions are distinct, they are

744 often required to be carried out in tandem, as respiration commonly follows fermentation for
745 yeast. It is possible that sensing and signaling pathways such as the Ras/PKA pathway evolved
746 to affect them together. This might be a general feature of signaling pathways as they must shift
747 multiple functions and performances together and this ability then represents an attractive target
748 for adaptive genetic changes.

749

750 If pleiotropic adaptation is a feature of the Ras/PKA pathway, the prediction is that 2nd step
751 adaptive Ras/PKA pathway mutations will remain adaptively pleiotropic. This is indeed the case.
752 Second-step mutations in the Ras/PKA pathway, mainly arising in the *TOR1* background, do
753 improve both fermentation and respiration performances. A small number of second-step
754 adaptive mutations outside of this pathway, in *ARO80* and *GSH1*, are also pleiotropically
755 adaptive and improve both respiration and fermentation, but to a smaller degree than Ras/PKA
756 pathway mutants. This suggests that the Ras/PKA pathway is virtually unique in its ability to
757 modulate both fermentation and respiration performances together to a substantial degree in an
758 adaptive manner, a notion also supported by the fact that we observe the shift towards
759 modularity adaptation already in the second adaptive step.

760

761 A small number of adaptive clones in the second step improved both fermentation and
762 respiration performances to a substantial degree. Sequencing of these clones showed that they
763 acquired multiple mutations, and several of these clones improved both performances by the
764 addition of two or more orthogonal steps. This suggests that adaptation can continue improving
765 both performances but the adaptive walk needs to engage multiple modules and multiple
766 mutations, making such adaptation slower than the first step of adaptation. This might be part of
767 the reason why adaptation in general slows down over the course of evolution (Wiser, Ribeck,
768 and Lenski 2013; Johnson et al. 2021; Good and Desai 2015; Aggeli, Li, and Sherlock 2021).

769

770 We argue that signaling pathways such as Ras/PKA have the capacity of generating “coherent
771 pleiotropy”, where the output of many cellular processes can be affected without disrupting the
772 proper regulation and function of each process. As such, signaling pathways that have been
773 evolutionarily pre-wired to control combinations of selective pressures may be easily modified
774 by mutation to coherently improve the performances under selection. The ability of signaling
775 pathways to generate coherent pleiotropy implies that many adaptive mutations should hit
776 signaling pathways. Indeed, this is what we see. For example, in cancer, the key oncogenes are
777 located along cellular signaling pathways and engage either receptors of signals or represent
778 key relay stations in these pathways (Bailey et al. 2018; Sanchez-Vega et al. 2018; Pawson and
779 Warner 2007; Sondka et al. 2018; Hanahan and Weinberg 2011; Hanahan 2022).

780

781 On the other hand, this coherent pleiotropy of signaling pathways does not necessarily indicate
782 that such mutations have no costs in other traits. Indeed, we see that many of the Ras/PKA
783 mutants exhibit costs in stationary phase. Moreover, in previous work, we find that the Ras/PKA
784 mutants have additional phenotypic effects with minor contributions to fitness in the Evo2D
785 evolution condition but substantial effects in other conditions (Kinsler, Geiler-Samerotte, and

786 Petrov 2020). Thus, we might expect these signaling pathways to be most likely to be targeted
787 by adaptation in relatively simple environments where the beneficial pleiotropic effects can be
788 realized with only minor other costs.

789

790 In addition to cellular signaling pathways, other gene-regulatory, hormonal, and neuronal
791 systems allow for organisms to be phenotypically plastic and involve coherent control of many
792 traits of an organism. As such, these systems may also be attractive targets for evolutionary
793 change, as they can serve as high-leverage routes for altering many traits simultaneously. The
794 evolution of phenotypic plasticity hence paves the way for subsequent large-effect evolutionary
795 shifts in local adaptation.

796

797 Finally, we believe that the existence of these high-leverage pleiotropic routes of adaptation
798 must be incorporated into our thinking of the evolution of complex systems. Indeed, we
799 commonly think of pleiotropy as purely random, with mutations shifting multiple traits at once in
800 a random and thus largely incoherent way. This generates expectations that pleiotropy should
801 be costly, as such incoherent shifts lead to a generically disorganized state. Given that actual
802 organisms have low-dimensional but pleiotropic signaling and regulatory systems, pleiotropy
803 can often be coherent and thus might often enhance adaptive potential and allow for surprisingly
804 large-effect adaptive mutations. It is therefore important to think of regulation and adaptation as
805 two sides of the same problem of how to change complex and tightly integrated systems in an
806 adaptive manner.

807 REFERENCES

- 808 Aggeli, Dimitra, Yuping Li, and Gavin Sherlock. 2021. "Changes in the Distribution of Fitness Effects and
809 Adaptive Mutational Spectra Following a Single First Step towards Adaptation." *Nature Communications* 12 (1): 5193. <https://doi.org/10.1038/s41467-021-25440-7>.
- 810 Ait-EI-Mkadem, Samira, Manal Dayem-Quere, Mirjana Gusic, Annabelle Chaussenot, Sylvie Bannwarth,
811 Bérengère François, Emmanuelle C. Genin, et al. 2017. "Mutations in MDH2, Encoding a Krebs
812 Cycle Enzyme, Cause Early-Onset Severe Encephalopathy." *American Journal of Human Genetics*
813 100 (1): 151–59. <https://doi.org/10.1016/j.ajhg.2016.11.014>.
- 814 Altschul, S. F., W. Gish, W. Miller, E. W. Myers, and D. J. Lipman. 1990. "Basic Local Alignment Search
815 Tool." *Journal of Molecular Biology* 215 (3): 403–10. [https://doi.org/10.1016/S0022-2836\(05\)80360-2](https://doi.org/10.1016/S0022-2836(05)80360-2).
- 816 Bailey, Matthew H., Collin Tokheim, Eduard Porta-Pardo, Sohini Sengupta, Denis Bertrand, Amila
817 Weerasinghe, Antonio Colaprico, et al. 2018. "Comprehensive Characterization of Cancer Driver
818 Genes and Mutations." *Cell* 173 (2): 371–85.e18. <https://doi.org/10.1016/j.cell.2018.02.060>.
- 819 Bakerlee, Christopher W., Angela M. Phillips, Alex N. Nguyen Ba, and Michael M. Desai. 2021.
820 "Dynamics and Variability in the Pleiotropic Effects of Adaptation in Laboratory Budding Yeast
821 Populations." *eLife* 10 (October). <https://doi.org/10.7554/eLife.70918>.
- 822 *BarcodeCounter2: Count DNA Barcodes Version 2.* n.d. Github. Accessed April 10, 2024.
823 <https://github.com/sandeepvenkataram/BarcodeCounter2>.
- 824 Blount, Zachary D., Christina Z. Borland, and Richard E. Lenski. 2008. "Historical Contingency and the
825 Evolution of a Key Innovation in an Experimental Population of *Escherichia Coli*." *Proceedings of the
826 National Academy of Sciences of the United States of America* 105 (23): 7899–7906.
827 <https://doi.org/10.1073/pnas.0803151105>.
- 828 Boles Eckhard, de Jong-Gubbels Patricia, and Pronk Jack T. 1998. "Identification and Characterization
829 of MAE1, the *Saccharomyces Cerevisiae* Structural Gene Encoding Mitochondrial Malic Enzyme."
830 *Journal of Bacteriology* 180 (11): 2875–82. <https://doi.org/10.1128/jb.180.11.2875-2882.1998>.
- 831 Bono, Lisa M., Leno B. Smith Jr, David W. Pfennig, and Christina L. Burch. 2017. "The Emergence of
832 Performance Trade-Offs during Local Adaptation: Insights from Experimental Evolution." *Molecular
833 Ecology* 26 (7): 1720–33. <https://doi.org/10.1111/mec.13979>.
- 834 Brown, James A., Gavin Sherlock, Chad L. Myers, Nicola M. Burrows, Changchun Deng, H. Irene Wu,
835 Kelly E. McCann, Olga G. Troyanskaya, and J. Martin Brown. 2006. "Global Analysis of Gene
836 Function in Yeast by Quantitative Phenotypic Profiling." *Molecular Systems Biology* 2 (January):
837 2006.0001. <https://doi.org/10.1038/msb4100043>.
- 838 Chaithanya, Koppisetty Viswa, and Himanshu Sinha. 2023. "MKT1 Alleles Regulate Stress Responses
839 through Posttranscriptional Modulation of Puf3 Targets in Budding Yeast." *Yeast* 40 (12): 616–27.
840 <https://doi.org/10.1002/yea.3908>.
- 841 Chang, Yeonji, and Won-Ki Huh. 2018. "Ksp1-Dependent Phosphorylation of eIF4G Modulates Post-
842 Transcriptional Regulation of Specific mRNAs under Glucose Deprivation Conditions." *Nucleic Acids
843 Research* 46 (6): 3047–60. <https://doi.org/10.1093/nar/gky097>.
- 844 Chou, Hsin-Hung, Hsuan-Chao Chiu, Nigel F. Delaney, Daniel Segrè, and Christopher J. Marx. 2011.
845 "Diminishing Returns Epistasis among Beneficial Mutations Decelerates Adaptation." *Science* 332
846 (6034): 1190–92. <https://doi.org/10.1126/science.1203799>.
- 847 Cingolani, Pablo, Adrian Platts, Le Lily Wang, Melissa Coon, Tung Nguyen, Luan Wang, Susan J. Land,
848 Xiangyi Lu, and Douglas M. Ruden. 2012. "A Program for Annotating and Predicting the Effects of
849 Single Nucleotide Polymorphisms, SnpEff: SNPs in the Genome of *Drosophila Melanogaster* Strain
850 w1118; Iso-2; Iso-3." *Fly* 6 (2): 80–92. <https://doi.org/10.4161/fly.19695>.
- 851 DeRisi, J. L., V. R. Iyer, and P. O. Brown. 1997. "Exploring the Metabolic and Genetic Control of Gene
852 Expression on a Genomic Scale." *Science* 278 (5338): 680–86.
853 <https://doi.org/10.1126/science.278.5338.680>.
- 854 Fisher, Kaitlin J., Sean W. Buskirk, Ryan C. Vignogna, Daniel A. Marad, and Gregory I. Lang. 2018.
855 "Adaptive Genome Duplication Affects Patterns of Molecular Evolution in *Saccharomyces
856 Cerevisiae*." *PLoS Genetics* 14 (5): e1007396. <https://doi.org/10.1371/journal.pgen.1007396>.
- 857 Good, Benjamin H., and Michael M. Desai. 2015. "The Impact of Macroscopic Epistasis on Long-Term
858

- 859 Evolutionary Dynamics." *Genetics* 199 (1): 177–90. <https://doi.org/10.1534/genetics.114.172460>.
- 860 Gupta, Saumya, Aparna Radhakrishnan, Pandu Raharja-Liu, Gen Lin, Lars M. Steinmetz, Julien
861 Gagneur, and Himanshu Sinha. 2015. "Temporal Expression Profiling Identifies Pathways Mediating
862 Effect of Causal Variant on Phenotype." *PLoS Genetics* 11 (6): e1005195.
863 <https://doi.org/10.1371/journal.pgen.1005195>.
- 864 Hanahan, Douglas. 2022. "Hallmarks of Cancer: New Dimensions." *Cancer Discovery* 12 (1): 31–46.
865 <https://doi.org/10.1158/2159-8290.CD-21-1059>.
- 866 Hanahan, Douglas, and Robert A. Weinberg. 2011. "Hallmarks of Cancer: The next Generation." *Cell* 144
867 (5): 646–74. <https://doi.org/10.1016/j.cell.2011.02.013>.
- 868 Harms, Michael J., and Joseph W. Thornton. 2014. "Historical Contingency and Its Biophysical Basis in
869 Glucocorticoid Receptor Evolution." *Nature* 512 (7513): 203–7. <https://doi.org/10.1038/nature13410>.
- 870 Hartwell, L. H., J. J. Hopfield, S. Leibler, and A. W. Murray. 1999. "From Molecular to Modular Cell
871 Biology." *Nature* 402 (6761 Suppl): C47–52. <https://doi.org/10.1038/35011540>.
- 872 Hong, Jungeui, and David Gresham. 2014. "Molecular Specificity, Convergence and Constraint Shape
873 Adaptive Evolution in Nutrient-Poor Environments." *PLoS Genetics* 10 (1): e1004041.
874 <https://doi.org/10.1371/journal.pgen.1004041>.
- 875 Iraqui, I., S. Vissers, B. André, and A. Urrestarazu. 1999. "Transcriptional Induction by Aromatic Amino
876 Acids in *Saccharomyces Cerevisiae*." *Molecular and Cellular Biology* 19 (5): 3360–71.
877 <https://doi.org/10.1128/MCB.19.5.3360>.
- 878 Jasmin, Jean-Nicolas, and Rees Kassen. 2007. "On the Experimental Evolution of Specialization and
879 Diversity in Heterogeneous Environments." *Ecology Letters* 10 (4): 272–81.
880 <https://doi.org/10.1111/j.1461-0248.2007.01021.x>.
- 881 Johnson, Milo S., Shreyas Gopalakrishnan, Juhee Goyal, Megan E. Dillingham, Christopher W. Bakerlee,
882 Parris T. Humphrey, Tanush Jagdish, et al. 2021. "Phenotypic and Molecular Evolution across
883 10,000 Generations in Laboratory Budding Yeast Populations." *eLife* 10 (January).
884 <https://doi.org/10.7554/eLife.63910>.
- 885 Kinsler, Grant, Kerry Geiler-Samerotte, and Dmitri A. Petrov. 2020. "Fitness Variation across Subtle
886 Environmental Perturbations Reveals Local Modularity and Global Pleiotropy of Adaptation." *eLife* 9
887 (December). <https://doi.org/10.7554/eLife.61271>.
- 888 Kinsler, Grant, Kara Schmidlin, Daphne Newell, Rachel Eder, Sam Apodaca, Grace Lam, Dmitri Petrov,
889 and Kerry Geiler-Samerotte. 2023. "Extreme Sensitivity of Fitness to Environmental Conditions:
890 Lessons from #1BigBatch." *Journal of Molecular Evolution* 91 (3): 293–310.
891 <https://doi.org/10.1007/s00239-023-10114-3>.
- 892 Kistler, M., K. Maier, and F. Eckardt-Schupp. 1990. "Genetic and Biochemical Analysis of Glutathione-
893 Deficient Mutants of *Saccharomyces Cerevisiae*." *Mutagenesis* 5 (1): 39–44.
894 <https://doi.org/10.1093/mutage/5.1.39>.
- 895 Komeili, A., K. P. Wedaman, E. K. O'Shea, and T. Powers. 2000. "Mechanism of Metabolic Control.
896 Target of Rapamycin Signaling Links Nitrogen Quality to the Activity of the Rtg1 and Rtg3
897 Transcription Factors." *The Journal of Cell Biology* 151 (4): 863–78.
898 <https://doi.org/10.1083/jcb.151.4.863>.
- 899 Kryazhimskiy, Sergey, Daniel P. Rice, Elizabeth R. Jerison, and Michael M. Desai. 2014. "Microbial
900 Evolution. Global Epistasis Makes Adaptation Predictable despite Sequence-Level Stochasticity."
901 *Science* 344 (6191): 1519–22. <https://doi.org/10.1126/science.1250939>.
- 902 Kurita, O., and Y. Nishida. 1999. "Involvement of Mitochondrial Aldehyde Dehydrogenase ALD5 in
903 Maintenance of the Mitochondrial Electron Transport Chain in *Saccharomyces Cerevisiae*." *FEMS
904 Microbiology Letters* 181 (2): 281–87. <https://doi.org/10.1111/j.1574-6968.1999.tb08856.x>.
- 905 Langmead, Ben, and Steven L. Salzberg. 2012. "Fast Gapped-Read Alignment with Bowtie 2." *Nature
906 Methods* 9 (4): 357–59. <https://doi.org/10.1038/nmeth.1923>.
- 907 Lapointe, Christopher P., Jonathan A. Stefely, Adam Jochem, Paul D. Hutchins, Gary M. Wilson, Nicholas
908 W. Kwiecien, Joshua J. Coon, Marvin Wickens, and David J. Pagliarini. 2018. "Multi-Omics Reveal
909 Specific Targets of the RNA-Binding Protein Puf3p and Its Orchestration of Mitochondrial
910 Biogenesis." *Cell Systems* 6 (1): 125–35.e6. <https://doi.org/10.1016/j.cels.2017.11.012>.
- 911 Lee, Chien-Der, and Benjamin P. Tu. 2015. "Glucose-Regulated Phosphorylation of the PUF Protein Puf3

- Regulates the Translational Fate of Its Bound mRNAs and Association with RNA Granules." *Cell Reports* 11 (10): 1638–50. <https://doi.org/10.1016/j.celrep.2015.05.014>.
- Lee, Kyusung, and Ji-Sook Hahn. 2013. "Interplay of Aro80 and GATA Activators in Regulation of Genes for Catabolism of Aromatic Amino Acids in *Saccharomyces Cerevisiae*." *Molecular Microbiology* 88 (6): 1120–34. <https://doi.org/10.1111/mmi.12246>.
- Levy, Sasha F., Jamie R. Blundell, Sandeep Venkataram, Dmitri A. Petrov, Daniel S. Fisher, and Gavin Sherlock. 2015. "Quantitative Evolutionary Dynamics Using High-Resolution Lineage Tracking." *Nature* 519 (7542): 181–86. <https://doi.org/10.1038/nature14279>.
- Liao, X., and R. A. Butow. 1993. "RTG1 and RTG2: Two Yeast Genes Required for a Novel Path of Communication from Mitochondria to the Nucleus." *Cell* 72 (1): 61–71. [https://doi.org/10.1016/0092-8674\(93\)90050-z](https://doi.org/10.1016/0092-8674(93)90050-z).
- Li, Fangfei, Aditya Mahadevan, and Gavin Sherlock. 2023. "An Improved Algorithm for Inferring Mutational Parameters from Bar-Seq Evolution Experiments." *BMC Genomics* 24 (1): 246. <https://doi.org/10.1186/s12864-023-09345-x>.
- Li, Fangfei, Jason Tarkington, and Gavin Sherlock. 2023. "Fit-Seq2.0: An Improved Software for High-Throughput Fitness Measurements Using Pooled Competition Assays." *Journal of Molecular Evolution* 91 (3): 334–44. <https://doi.org/10.1007/s00239-023-10098-0>.
- Li, Heng. 2011. "A Statistical Framework for SNP Calling, Mutation Discovery, Association Mapping and Population Genetical Parameter Estimation from Sequencing Data." *Bioinformatics* 27 (21): 2987–93. <https://doi.org/10.1093/bioinformatics/btr509>.
- Li, Heng, and Richard Durbin. 2009. "Fast and Accurate Short Read Alignment with Burrows–Wheeler Transform." *Bioinformatics* 25 (14): 1754–60. <https://doi.org/10.1093/bioinformatics/btp324>.
- Liu, Zhengchang, Takayuki Sekito, Mário Spírek, Janet Thornton, and Ronald A. Butow. 2003. "Retrograde Signaling Is Regulated by the Dynamic Interaction between Rtg2p and Mks1p." *Molecular Cell* 12 (2): 401–11. [https://doi.org/10.1016/s1097-2765\(03\)00285-5](https://doi.org/10.1016/s1097-2765(03)00285-5).
- Li, Yuping, Dmitri A. Petrov, and Gavin Sherlock. 2019. "Single Nucleotide Mapping of Trait Space Reveals Pareto Fronts That Constrain Adaptation." *Nature Ecology & Evolution* 3 (11): 1539–51. <https://doi.org/10.1038/s41559-019-0993-0>.
- Li, Yuping, Sandeep Venkataram, Atish Agarwala, Barbara Dunn, Dmitri A. Petrov, Gavin Sherlock, and Daniel S. Fisher. 2018. "Hidden Complexity of Yeast Adaptation under Simple Evolutionary Conditions." *Current Biology: CB* 28 (4): 515–25.e6. <https://doi.org/10.1016/j.cub.2018.01.009>.
- McAlister-Henn, L., and L. M. Thompson. 1987. "Isolation and Expression of the Gene Encoding Yeast Mitochondrial Malate Dehydrogenase." *Journal of Bacteriology* 169 (11): 5157–66. <https://doi.org/10.1128/jb.169.11.5157-5166.1987>.
- Melo, Diogo, Arthur Porto, James M. Cheverud, and Gabriel Marroig. 2016. "Modularity: Genes, Development and Evolution." *Annual Review of Ecology, Evolution, and Systematics* 47 (September): 463–86. <https://doi.org/10.1146/annurev-ecolsys-121415-032409>.
- Murphy, J. Patrick, Ekaterina Stepanova, Robert A. Everley, Joao A. Paulo, and Steven P. Gygi. 2015. "Comprehensive Temporal Protein Dynamics during the Diauxic Shift in *Saccharomyces Cerevisiae*." *Molecular & Cellular Proteomics: MCP* 14 (9): 2454–65. <https://doi.org/10.1074/mcp.M114.045849>.
- Navarro-Aviño, J. P., R. Prasad, V. J. Miralles, R. M. Benito, and R. Serrano. 1999. "A Proposal for Nomenclature of Aldehyde Dehydrogenases in *Saccharomyces Cerevisiae* and Characterization of the Stress-Inducible ALD2 and ALD3 Genes." *Yeast* 15 (10A): 829–42. [https://doi.org/10.1002/\(SICI\)1097-0061\(199907\)15:10A<829::AID-YEA423>3.0.CO;2-9](https://doi.org/10.1002/(SICI)1097-0061(199907)15:10A<829::AID-YEA423>3.0.CO;2-9).
- Orr, H. A. 2000. "Adaptation and the Cost of Complexity." *Evolution; International Journal of Organic Evolution* 54 (1): 13–20. <https://doi.org/10.1111/j.0014-3820.2000.tb00002.x>.
- Park, Yeonwoo, Brian P. H. Metzger, and Joseph W. Thornton. 2022. "Epistatic Drift Causes Gradual Decay of Predictability in Protein Evolution." *Science* 376 (6595): 823–30. <https://doi.org/10.1126/science.abn6895>.
- Pawson, T., and N. Warner. 2007. "Oncogenic Re-Wiring of Cellular Signaling Pathways." *Oncogene* 26 (9): 1268–75. <https://doi.org/10.1038/sj.onc.1210255>.
- Reinders, Jörg, Karina Wagner, Rene P. Zahedi, Diana Stojanovski, Beate Eyrich, Martin van der Laan, Peter Rehling, Albert Sickmann, Nikolaus Pfanner, and Chris Meisinger. 2007. "Profiling

- 965 Phosphoproteins of Yeast Mitochondria Reveals a Role of Phosphorylation in Assembly of the ATP
966 Synthase*." *Molecular & Cellular Proteomics: MCP* 6 (11): 1896–1906.
967 <https://doi.org/10.1074/mcp.M700098-MCP200>.
- 968 Repetto, B., and A. Tzagoloff. 1989. "Structure and Regulation of KGD1, the Structural Gene for Yeast
969 Alpha-Ketoglutarate Dehydrogenase." *Molecular and Cellular Biology* 9 (6): 2695–2705.
970 <https://doi.org/10.1128/mcb.9.6.2695-2705.1989>.
- 971 Sanchez-Vega, Francisco, Marco Mina, Joshua Armenia, Walid K. Chatila, Augustin Luna, Konnor C. La,
972 Sofia Dimitriadou, et al. 2018. "Oncogenic Signaling Pathways in The Cancer Genome Atlas." *Cell*
973 173 (2): 321–37.e10. <https://doi.org/10.1016/j.cell.2018.03.035>.
- 974 Schlossarek, Dennis, Marcin Luzarowski, Ewelina M. Sokołowska, Venkatesh P. Thirumalaikumar, Lisa
975 Dengler, Lothar Willmitzer, Jennifer C. Ewald, and Aleksandra Skirycz. 2022. "Rewiring of the
976 Protein-Protein-Metabolite Interactome during the Diauxic Shift in Yeast." *Cellular and Molecular Life
977 Sciences: CMLS* 79 (11): 550. <https://doi.org/10.1007/s00018-022-04569-8>.
- 978 Sekito, Takayuki, Zhengchang Liu, Janet Thornton, and Ronald A. Butow. 2002. "RTG-Dependent
979 Mitochondria-to-Nucleus Signaling Is Regulated by MKS1 and Is Linked to Formation of Yeast Prion
980 [URE3]." *Molecular Biology of the Cell* 13 (3): 795–804. <https://doi.org/10.1091/mbc.01-09-0473>.
- 981 Sekito, T., J. Thornton, and R. A. Butow. 2000. "Mitochondria-to-Nuclear Signaling Is Regulated by the
982 Subcellular Localization of the Transcription Factors Rtg1p and Rtg3p." *Molecular Biology of the Cell*
983 11 (6): 2103–15. <https://doi.org/10.1091/mbc.11.6.2103>.
- 984 Sondka, Zbyslaw, Sally Bamford, Charlotte G. Cole, Sari A. Ward, Ian Dunham, and Simon A. Forbes.
985 2018. "The COSMIC Cancer Gene Census: Describing Genetic Dysfunction across All Human
986 Cancers." *Nature Reviews. Cancer* 18 (11): 696–705. <https://doi.org/10.1038/s41568-018-0060-1>.
- 987 Suissa, M., K. Suda, and G. Schatz. 1984. "Isolation of the Nuclear Yeast Genes for Citrate Synthase and
988 Fifteen Other Mitochondrial Proteins by a New Screening Method." *The EMBO Journal* 3 (8): 1773–
989 81. <https://doi.org/10.1002/j.1460-2075.1984.tb02045.x>.
- 990 Tung, Sudipta, Christopher W. Bakerlee, Angela M. Phillips, Alex N. Nguyen Ba, and Michael M. Desai.
991 2021. "The Genetic Basis of Differential Autodiploidization in Evolving Yeast Populations." *G3* 11 (8).
992 <https://doi.org/10.1093/g3journal/jkab192>.
- 993 Umekawa, Midori, and Daniel J. Klionsky. 2012. "Ksp1 Kinase Regulates Autophagy via the Target of
994 Rapamycin Complex 1 (TORC1) Pathway." *The Journal of Biological Chemistry* 287 (20): 16300–
995 310. <https://doi.org/10.1074/jbc.M112.344952>.
- 996 Van der Auwera, Geraldine A., and Brian D. O'Connor. 2020. *Genomics in the Cloud: Using Docker,
997 GATK, and WDL in Terra*. "O'Reilly Media, Inc."
998 <https://play.google.com/store/books/details?id=vsXaDwAAQBAJ>.
- 999 Venkataram, Sandeep, Barbara Dunn, Yuping Li, Atish Agarwala, Jessica Chang, Emily R. Ebel, Kerry
1000 Geiler-Samerotte, et al. 2016. "Development of a Comprehensive Genotype-to-Fitness Map of
1001 Adaptation-Driving Mutations in Yeast." *Cell* 166 (6): 1585–96.e22.
1002 <https://doi.org/10.1016/j.cell.2016.08.002>.
- 1003 Wagner, Günter P., and Lee Altenberg. 1996. "PERSPECTIVE: COMPLEX ADAPTATIONS AND THE
1004 EVOLUTION OF EVOLVABILITY." *Evolution; International Journal of Organic Evolution* 50 (3): 967–
1005 76. <https://doi.org/10.1111/j.1558-5646.1996.tb02339.x>.
- 1006 Wagner, Günter P., Mihaela Pavlicev, and James M. Cheverud. 2007. "The Road to Modularity." *Nature
1007 Reviews. Genetics* 8 (12): 921–31. <https://doi.org/10.1038/nrg2267>.
- 1008 Wagner, Günter P., and Jianzhi Zhang. 2011. "The Pleiotropic Structure of the Genotype-Phenotype Map:
1009 The Evolvability of Complex Organisms." *Nature Reviews. Genetics* 12 (3): 204–13.
1010 <https://doi.org/10.1038/nrg2949>.
- 1011 Welch, John J., and David Waxman. 2003. "Modularity and the Cost of Complexity." *Evolution;
1012 International Journal of Organic Evolution* 57 (8): 1723–34. [https://doi.org/10.1111/j.0014-3820.2003.tb00581.x](https://doi.org/10.1111/j.0014-
1013 3820.2003.tb00581.x).
- 1014 Wilson, Wayne A., and Peter J. Roach. 2002. "Nutrient-Regulated Protein Kinases in Budding Yeast."
1015 *Cell* 111 (2): 155–58. [https://doi.org/10.1016/s0092-8674\(02\)01043-7](https://doi.org/10.1016/s0092-8674(02)01043-7).
- 1016 Wiser, Michael J., Noah Ribeck, and Richard E. Lenski. 2013. "Long-Term Dynamics of Adaptation in
1017 Asexual Populations." *Science* 342 (6164): 1364–67. <https://doi.org/10.1126/science.1243357>.

- 1018 Wünsche, Andrea, Duy M. Dinh, Rebecca S. Satterwhite, Carolina Diaz Arenas, Daniel M. Stoebel, and
1019 Tim F. Cooper. 2017. "Diminishing-Returns Epistasis Decreases Adaptability along an Evolutionary
1020 Trajectory." *Nature Ecology & Evolution* 1 (4): 61. <https://doi.org/10.1038/s41559-016-0061>.
- 1021 Zampar, Guillermo G., Anne Kümmel, Jennifer Ewald, Stefan Jol, Bastian Niebel, Paola Picotti, Ruedi
1022 Aebersold, Uwe Sauer, Nicola Zamboni, and Matthias Heinemann. 2013. "Temporal System-Level
1023 Organization of the Switch from Glycolytic to Gluconeogenic Operation in Yeast." *Molecular Systems
1024 Biology* 9: 651. <https://doi.org/10.1038/msb.2013.11>.

1025 **METHODS**

1026

1027 **Constructing barcoded populations from first-step mutants**

1028 To conduct second-step evolution experiments, we constructed barcoded populations for each
1029 of five mutations (see table 1) that arose in the original 2-Day evolution experiment (Levy et al.
1030 2015). Construction of the barcoded populations of *CYR1*, *GPB2*, and *TOR1* mutations was
1031 previously described (Aggeli, Li, and Sherlock 2021). To barcode *IRA1-nonsense* and *IRA1-*
1032 *missense* mutants, we followed a similar procedure. Specifically, we backcrossed the *IRA1*
1033 mutants (*MAT α*) to GSY5375, a *MAT α* ancestral S288C strain that harbors the pre-landing pad
1034 locus (Aggeli, Li, and Sherlock 2021). After sporulation and tetrad dissection, we performed
1035 Sanger sequencing to identify segregants that were *MAT α* , carried the *IRA1* variant of interest,
1036 and the pre-landing pad allele at the barcode locus, ensuring the removal of the barcode initially
1037 labeling this strain. These segregants were used for downstream transformation of barcodes.

1038

1039 We then barcoded these strains with a low and high complexity barcode as described in Aggeli
1040 et al. We first transformed in the low-complexity barcode by PCR-amplifying a region from the
1041 L001 library, which harbors a NatMX selectable marker, half of *URA3*, an artificial intron, a low-
1042 complexity barcode sequence, and a lox66 site. We then selected for successful transformants
1043 using YPD + Nat plates and isolated 4 and 8 colonies for *IRA1-missense* and *IRA1-nonsense*
1044 strains, respectively, each with a unique low-complexity barcode. For each of these strains, we
1045 then transformed a library of high-complexity barcodes (pBAR3). After transformation, cells
1046 were grown in YP + 2% galactose for 16hrs to induce Cre recombinase expression prior to
1047 selection on SC-ura plates with 2% glucose. We then estimated the number of unique
1048 transformants by counting the number of colonies grown from plating a dilution. We additionally
1049 estimated the relative number of unique transformants by amplicon Illumina sequencing using
1050 the sequencing primers described below.

1051

1052 To construct populations for evolution experiments, we pooled together transformants from
1053 multiple high-complexity transformations, such that each barcode was equally represented in
1054 each pool. This resulted in pools of ~100,000 high-complexity barcodes for each evolution
1055 experiment with the exception of Evo2D *IRA1-missense* evolution pool which contained ~40,000
1056 high-complexity barcodes. Transformants were pooled such that each low-complexity barcode
1057 was only present in one evolution pool, allowing us later to identify evolution conditions based
1058 on the identity of the low-complexity barcode. For Evo1D experiments, a pool of *IRA1-missense*
1059 and *IRA1-nonsense* transformants was used, containing equal numbers in abundance, albeit
1060 with ~32,000 unique *IRA1-missense* barcodes and ~60,000 *IRA1-nonsense* barcodes. A single
1061 pool that contained barcoded populations of *CYR1*, *GPB2*, and *TOR1* mutants was used for the
1062 second-step Evo1D and Evo3D experiments for these genotypes.

1063

1064 **Conducting evolution experiments.**

1065 We conducted evolution experiments with barcoded populations under identical conditions to
1066 the original evolution experiment. Briefly, ~10^8 cells of each evolution population pool was

1067 inoculated in 50 mL of SC-ura + 2% dextrose + hygromycin in 500 mL Delong flasks and grown
1068 overnight at 30°C with shaking at 223 rpm. 500 µL of saturated overnight culture was then
1069 transferred to 100 mL of glucose-limited M3 medium (5x delft medium with 4% ammonium
1070 sulfate and 1.5% dextrose) in 500 mL Delong flasks for the evolution experiment. For most of
1071 the evolution experiments, the culture was split into 2 replicate flasks at this point. Second-step
1072 Evo3D experiments from *IRA1-missense* or *IRA1-nonsense* mutants used 3 replicates each.
1073 Cultures then propagated every 24, 48, or 72 hours for Evo1D, Evo2D, and Evo3D conditions,
1074 respectively. At the time of transfer, a set volume was transferred into 100 mL of fresh medium.
1075 In order to keep the bottleneck size consistent at ~5x10⁷ viable cells, the volume varied by
1076 condition. Evo2D conditions used 400 µl of transfer volume. Evo1D and Evo3D conditions used
1077 500 µL of transfer volume, which accounted for decreased cell density and decreased cell
1078 viability in these conditions, respectively. Two 1 mL volumes of saturated culture were frozen as
1079 glycerol stocks. The remaining culture was spun down, resuspended in 5 mL of sorbitol freezing
1080 solution (0.9M sorbitol, 100mM Tris pH 7.5, 100mM EDTA) and frozen at -20°C for subsequent
1081 genomic DNA extraction and barcode library sequencing preparation.

1082

1083 Isolation of clones from evolution experiments.

1084

1085 To isolate clones for fitness measurement experiments, quantification of growth phase
1086 performances, and whole genome sequencing, we sorted individual cells as previously
1087 described (Y. Li, Petrov, and Sherlock 2019) . Specifically, we sorted 480 individual cells (five
1088 96-well plates) from each replicate evolution experiment into single wells of a 96-well plate with
1089 100 µL of YPD medium. This resulted in a total of 80 plates (~7,680 sorted cells) across the 16
1090 evolution experiments. Sorted cells were then grown at 30°C for 3 days without shaking until the
1091 cells reached saturation. Saturated cultures (5µl) were then transferred to deep-well 96-well
1092 plates with 300 µL of YPD. After 2 days of growth at 30°C without shaking, 100 µL of culture
1093 were mixed with glycerol and frozen at -80°C. 20 µL of saturated culture were transferred to 96-
1094 well PCR plates and frozen at -20°C. for barcode identification. Saturated culture was also
1095 plated onto Benomyl plates to assay ploidy (Venkataram et al. 2016).

1096

1097 Barcode identification by Metagrid.

1098 To identify the barcode associated with each well and ensure that multiple clones with the same
1099 barcode were not kept for downstream fitness measurement experiments, we performed
1100 sequencing on the barcodes of the clones in each well. Saturated culture (20µl) was transferred
1101 to 96-well plates and frozen at -20°C. Cells were then lysed by incubation at 95°C for 15 min. 5
1102 µL of lysed culture were used as the template for PCR amplification of the barcode region. We
1103 performed two steps of PCR. In the first-step of PCR, we used a set of 72 forward and 64
1104 reverse first-step primers, each with a unique 8-bp multiplexing tag, to combinatorially label
1105 each well. After the first-step of PCR, 5 µL of each well's PCR product from 5 plates was pooled
1106 together and the appropriate 250bp band was isolated using gel purification. A second-step of
1107 PCR was then performed with standard Nextera primers. Amplicon libraries were then
1108 sequenced on Illumina MiSeq or HiSeq machines.

1109
1110 To computationally identify the barcodes associated with each well, we used BarcodeCounter2
1111 to extract the multiplexing indexes and barcode regions from each read. We then associated
1112 barcodes with each well by taking the barcode with the most reads per well, provided the well
1113 had at least 200 reads, the barcode was at least 60% of the well's reads, and it received more
1114 than 1.5x the second-highest barcode in the well. This resulted in identifying the locations of
1115 1785 unique barcoded clones. This is lower than the highest possible number of 7,680 clones
1116 due to a combination of some wells receiving multiple clones, multiple wells receiving cells of
1117 the same barcode, and drop out due to sequencing depth. To further validate our approach, we
1118 randomly selected 3 wells per plate and performed Sanger sequencing of their barcodes. Of the
1119 wells where both barcodes were identified using the metagrid approach and Sanger reads were
1120 of sufficiently high quality, over 85% of the barcodes matched. We subsequently pooled each
1121 uniquely barcoded clone by evolution condition and parental strain, resulting in 4 pools of
1122 barcoded lineages to be used for fitness measurement experiments.
1123

1124 *Benomyl ploidy test.*
1125 To characterize the ploidy of each sorted clone, we performed a high-throughput ploidy test that
1126 was previously developed (Venkataram et al. 2016). Saturated culture from cell sorting was
1127 pinned onto YPD agar plates containing 20 mg/mL benomyl. Plates were then grown at 25°C for
1128 2 days and then imaged. Clones with inhibited growth on the benomyl medium were identified
1129 as diploids. Clones with normal growth on the benomyl medium were identified as haploids. See
1130 "Mutation and ploidy classification" section below.
1131

1132 **Constructing barcoded pools**
1133 To construct a pool of lineages for fitness measurement experiments, we generated one large
1134 pool of barcoded lineages isolated from previous evolution experiments and the evolution
1135 experiments described in this study. Briefly, one tube of each barcode pool was thawed and
1136 grown in YPD at 30°C overnight. After the overnight growth, we pooled all barcode-sub pools
1137 together, adjusting for the number of barcodes in each pool and the OD600 of the culture, such
1138 that each barcode was equally represented in this big pool. This big pool was then split into 1
1139 mL glycerol stock aliquots and frozen at -80°C.
1140

1141 To precisely measure the mean fitness of the population, we constructed two pools of 60 neutral
1142 lineages from Venkataram 2016 and Li 2019. Briefly, we identified barcodes that exhibited
1143 neutral fitness estimates across all previous experiments done with these pools of barcoded
1144 lineages (Venkataram et al. 2016; Y. Li et al. 2018; Y. Li, Petrov, and Sherlock 2019; Kinsler,
1145 Geiler-Samerotte, and Petrov 2020). We then streaked out from glycerol stocks onto YPD
1146 plates. A single colony was picked from each barcoded lineage and grown in 96-well deep-well
1147 plates for 2 days. Wells for each collection of 60 neutrals were then pooled equally by volume.
1148 Then, glycerol stocks were created with 1 mL of pooled culture and frozen at -80°C.

1149
1150 **Fitness measurement experiments**
1151 To quantify fitness effects, we performed fitness measurement experiments. We streaked out
1152 DPY256 (an ancestor strain which harbors an ApaLI restriction site in the barcode region) onto
1153 a YPD plate. After two days of growth, a colony was picked and grown up in 50 mL of YPD
1154 overnight. Additionally, one tube each of the 60-neutral pool from Venkataram 2016 and one
1155 tube of the 60-neutral pool from the Li 2019 pool was thawed and grown separately in 50 mL of
1156 YPD overnight.
1157
1158 5x10⁷ cells from DPY256 ancestor, each of the two neutral pools, and the big pool (see
1159 Constructing barcoded pools) were then separately inoculated into four 500 mL Delong flasks
1160 containing 100 mL of M3 medium for one cycle of pre-culture in the selective condition. This
1161 resulted in a total of 16 flasks of culture, corresponding to each set of barcoded cells and the
1162 four conditions.
1163
1164 After one cycle of growth (which corresponded to 24h for the 1-Day transfer condition, 48h for 2-
1165 Day, 72h for 3-Day, and 120h for 5-Day), the cultures were pooled by volume such that the big
1166 pool of barcoded lineages represented 2% or 5% of the population. In the 2% flasks, 2% of the
1167 population was the big pool of evolved lineages, 2% were Venkataram 2016 neutrals, 2% were
1168 Li 2019 neutrals, and 94% of the population was DPY256 ancestor. In the 5% flasks, 5% of the
1169 population was the big pool of evolved lineages, 2% were Venkataram 2016 neutrals, 2% were
1170 Li 2019 neutrals, and 91% of the population was DPY256 ancestor. These pools of lineages is
1171 considered “Timepoint 0” for each condition and pooling percentage.
1172
1173 We then transferred a set volume of this pool to replicate flasks (2 replicates for 1- and 2-Day
1174 experiments, 3 replicates for 3- and 5-Day experiments) containing 100 mL M3 medium such
1175 that ~5x10⁷ of viable cells were transferred. This volume was 500 µL for 1-, 3-, and 5-Day
1176 experiments and 400 µL for 2-Day experiments. The culture was then grown at 30°C in an
1177 incubator shaking at 223 RPM. After the set amount of time corresponding to each condition, a
1178 fixed volume of culture (500 µL for 1-, 3-, and 5-Day experiments and 400 µL for 2-Day
1179 experiments) to fresh 100 mL of M3 medium in 500 mL DeLong flasks. This serial dilution was
1180 continued for until transfer 6 for 1- and 2-Day experiments and until transfer 2 for 3- and 5-Day
1181 experiments.
1182
1183 After each transfer, the remaining culture was frozen for downstream DNA extraction, barcode
1184 amplification, and sequencing. To freeze the culture, we transferred the culture to 50 mL conical
1185 tubes, spun down at 3000 rpm for 5 min, resuspending in 5 mL sorbitol freezing solution (0.9 M
1186 sorbitol, 0.1 M Tris-HCL pH 7.5, 0.1 M EDTA pH 8.0), aliquoted into three 1.5 mL tubes, and
1187 stored at -80°C.
1188

1189 **Genomic DNA extraction**
1190 Genomic DNA was extracted from frozen cells as described previously (Aggeli, Li, and Sherlock
1191 2021). Briefly, 400 μ L of frozen cells in sorbitol solution was spun down at 3500 rpm for 3 min.
1192 After discarding the supernatant, the cell pellet was then washed in 400 μ L of sterile water and
1193 spun down at 3500 rpm for 3 min and the supernatant was discarded. The cell pellet was then
1194 re-suspended in 400 μ L of extraction buffer (0.9 M sorbitol, 50 mM Na phosphate pH 7.5,
1195 240 μ g/mL zymolase, 14 mM β -mercaptoethanol) and incubated at 37°C for 30min. We then
1196 added 40 μ L of 0.5 M EDTA, 40 μ L of 10% SDS, and 56 μ L of proteinase K (Life Technologies
1197 25530-015), vortexing after each addition. The mixture was then incubated at 65°C for 30 min.
1198 After the incubation, tubes were placed on ice for 5 min and then 200 μ L of 5 M potassium
1199 acetate were added and tubes were shaken to mix. Following a 30 min incubation on ice, the
1200 samples were spun for 10 min at 17,000 rpm. The supernatant was transferred to a new 1.5 mL
1201 tube containing 750 μ L of isopropanol and placed on ice for 5 min. We then spun the samples at
1202 17,000 rpm for 10min and discarded the supernatant. The DNA pellet was then washed twice
1203 with 750 μ L 70% ethanol, each time vortexing very briefly, spun at 17,000 rpm for 2 min, and
1204 discarding the supernatant. After allowing the DNA pellet to dry completely, it was resuspended
1205 in 50 μ L 10 mM Tris ph 7.5 or 50 μ L nuclease free water. We then added 1 μ L of 20 mg/mL
1206 RNase A and subsequently incubated at 65°C for 30 min. DNA was then quantified using the
1207 Qubit Range dsDNA assay kit.

1208

1209 **Restriction digest of ancestral strain's barcode**

1210 Because over 90% of the initial population during the fitness measurement experiments consists
1211 of the ancestral strain, we sought to reduce the proportion of reads that represented its barcode
1212 to reduce sequencing costs. We thus performed restriction digestion using the ApaLI restriction
1213 site (GTGCAC) engineered into the barcode region of the DPY256 ancestral strain on DNA for
1214 each sample prior to (and following) PCR amplification. We added 1 μ L of ApaLI (NEB
1215 #R0507L) and 5.5 μ L of Cutsmart Buffer (NEB #R0507L) to genomic DNA and incubated at
1216 37°C for at least 1hr. Note that no barcode strains besides the ancestral strain contain this
1217 restriction site, due to the design of the barcode region.

1218

1219 **Barcode sequencing library preparation**

1220 To prepare sequencing libraries of the barcodes, we used a two-step PCR amplification
1221 protocol, as previously described (Venkataram et al. 2016; Kinsler, Geiler-Samerotte, and
1222 Petrov 2020; Y. Li et al. 2018). In the first step of PCR, we use HPLC-purified primers that
1223 contain “inline indices” to label samples and 8-bp Unique Molecular Identifiers (UMIs) to identify
1224 barcode reads from the same yeast cell that have been sequenced multiple times due to PCR
1225 amplification.

1226

1227 **Step 1 forward primers:**

F201	TCGTCGGCAGCGTC AGATGTGTATAAGAGACAG (N1:25252525)(N1)(N1) (N1)(N1)(N1)CGATGTT TAATATGGACTAAAGGAGGCTTT
F202	TCGTCGGCAGCGTC AGATGTGTATAAGAGACAG (N1:25252525)(N1)(N1) (N1)(N1)(N1) (N1)(N1)ACAGTGT TAATATGGACTAAAGGAGGCTTT
F203	TCGTCGGCAGCGTC AGATGTGTATAAGAGACAG (N1:25252525)(N1)(N1) (N1)(N1)(N1) (N1)(N1)TGACCAT TAATATGGACTAAAGGAGGCTTT
F204	TCGTCGGCAGCGTC AGATGTGTATAAGAGACAG (N1:25252525)(N1)(N1) (N1)(N1)(N1) (N1)(N1)GCCAATT TAATATGGACTAAAGGAGGCTTT
F205	TCGTCGGCAGCGTC AGATGTGTATAAGAGACAG (N1:25252525)(N1)(N1) (N1)(N1)(N1) (N1)(N1)ATCACGT TAATATGGACTAAAGGAGGCTTT

F206	TCGTCGGCAGCGTC AGATGTGTATAAGAGACAG (N1:25252525)(N1)(N1) (N1)(N1)(N1)CAGATCT TAATATGGACTAAAGGAGGCTTT
F207	TCGTCGGCAGCGTC AGATGTGTATAAGAGACAG (N1:25252525)(N1)(N1) (N1)(N1)(N1)GGCTACT TAATATGGACTAAAGGAGGCTTT
F208	TCGTCGGCAGCGTC AGATGTGTATAAGAGACAG (N1:25252525)(N1)(N1) (N1)(N1)(N1)TAGCTT TAATATGGACTAAAGGAGGCTTT
F209	TCGTCGGCAGCGTC AGATGTGTATAAGAGACAG (N1:25252525)(N1)(N1) (N1)(N1)(N1)N1TAGGGCT TAATATGGACTAAAGGAGGCTTT
F210	TCGTCGGCAGCGTC AGATGTGTATAAGAGACAG (N1:25252525)(N1)(N1) (N1)(N1)(N1)N1ACTGGAT TAATATGGACTAAAGGAGGCTTT
F211	TCGTCGGCAGCGTC AGATGTGTATAAGAGACAG (N1:25252525)(N1)(N1) (N1)(N1)(N1)N1GATCACT TAATATGGACTAAAGGAGGCTTT
F212	TCGTCGGCAGCGTC AGATGTGTATAAGAGACAG (N1:25252525)(N1)(N1) (N1)(N1)(N1)N1CTTGAT TAATATGGACTAAAGGAGGCTTT

1228

1229 Step 1 reverse primers:

R301	GTCTCGTGGGCTCGG AGATGTGTATAAGAGACAG (N1:25252525)(N1)(N1) (N1)(N1)(N1)TATATACGC TCGAATTCAAGCTTAGATCTGATA
R302	GTCTCGTGGGCTCGG AGATGTGTATAAGAGACAG (N1:25252525)(N1)(N1) (N1)(N1)(N1)CGCTCTATC TCGAATTCAAGCTTAGATCTGATA
R303	GTCTCGTGGGCTCGG AGATGTGTATAAGAGACAG (N1:25252525)(N1)(N1) (N1)(N1)(N1)N1GAGACGCTCT CGAATTCAAGCTTAGATCTGATA
R304	GTCTCGTGGGCTCGG AGATGTGTATAAGAGACAG (N1:25252525)(N1)(N1) (N1)(N1)(N1)N1ATACTGCGT TCGAATTCAAGCTTAGATCTGATA
R305	GTCTCGTGGGCTCGG AGATGTGTATAAGAGACAG (N1:25252525)(N1)(N1) (N1)(N1)(N1)N1ACTACGAGA TCGAATTCAAGCTTAGATCTGATA
R306	GTCTCGTGGGCTCGG AGATGTGTATAAGAGACAG (N1:25252525)(N1)(N1) (N1)(N1)(N1)N1TGAGCTAGC TCGAATTCAAGCTTAGATCTGATA
R307	GTCTCGTGGGCTCGG AGATGTGTATAAGAGACAG (N1:25252525)(N1)(N1) (N1)(N1)(N1)N1CTGCTACTC TCGAATTCAAGCTTAGATCTGATA
R308	GTCTCGTGGGCTCGG AGATGTGTATAAGAGACAG (N1:25252525)(N1)(N1) (N1)(N1)(N1)N1CGCTACGCA TCGAATTCAAGCTTAGATCTGATA

1230

1231 For the first step for PCR, we performed 8 or 16 reactions per sample, using ~4.8ug (ranging
 1232 between 3ug and 7.5ug) of DNA per sample across all reactions. Each set of eight 50 μ L
 1233 reactions included 16 μ l of 50mM MgCl₂, 8 μ L of 10 μ M forward primer, 8 μ L of 10 μ M reverse
 1234 primer, template DNA, and 200 μ L of OneTaq HotStart 2X Master mix (NEB #M0484L). Three
 1235 cycles of PCR was then carried out with the following steps:

1. 94°C for 10min
2. 94°C for 3min
3. 55°C for 1min
4. 68°C for 1 min
5. Repeat steps 2-4 twice for a total of 3 cycles
6. 68°C for 1min
7. Hold at 4°C

1236

1237 The first-step PCR product was then column purified using the GeneJET Gel Extraction Kit
 1238 (#K0692). Briefly, 100 μ L of orange binding buffer were added to each 50 μ L reaction. All 8 or
 1239 16 reactions from a given sample were pooled into the same purification column in a vacuum
 1240 manifold. We then washed the column with 750 μ L of wash buffer over vacuum. Then, each
 1241 column was spun for 30s at max speed to remove residual wash buffer. We then eluted into 47
 1242 μ L of nuclease free water by centrifuging and stored the samples at 4°C for the second step of
 1243 PCR.

1244

1245 The second step of PCR further amplifies the barcodes and attaches Illumina indices as well as
 1246 P5, P7 sequences for compatibility with Illumina sequencing, as done previously (Kinsler,
 1247 Geiler-Samerotte, and Petrov 2020; Kinsler et al. 2023). We used Nextera Index Xt v2 primers
 1248 (Illumina #FC-131–2004) with the following sequences:

1249

S513	AATGATACGGCGACCACCGAGATCTACACTCGACTAGTCGTCGGCAGCGTC
S515	AATGATACGGCGACCACCGAGATCTACACTTCAGCTCGTCGGCAGCGTC
S516	AATGATACGGCGACCACCGAGATCTACACCCCTAGAGTCGTCGGCAGCGTC
S517	AATGATACGGCGACCACCGAGATCTACACCGCTAAGATCGTCGGCAGCGTC
S518	AATGATACGGCGACCACCGAGATCTACACCTATTAAGTCGTCGGCAGCGTC

S520	AATGATAACGGCACCACCGAGATCTACACAAGGCTATTCTCGGCAGCGTC
S521	AATGATAACGGCACCACCGAGATCTACACGAGCCTTATCGTCGGCAGCGTC
S522	AATGATAACGGCACCACCGAGATCTACACTTATCGCATCGTCGGCAGCGTC
N716	CAAGCAGAAGACGGCATACGAGATTAGCGAGTGTCTCGTGGGCTCGG
N718	CAAGCAGAAGACGGCATACGAGATGTAGCTCCGTCTCGTGGGCTCGG
N719	CAAGCAGAAGACGGCATACGAGATTACTACCGGTCTCGTGGGCTCGG
N720	CAAGCAGAAGACGGCATACGAGATAGGCTCCGTCTCGTGGGCTCGG
N721	CAAGCAGAAGACGGCATACGAGATGCGAGCTCGTGGGCTCGG
N722	CAAGCAGAAGACGGCATACGAGATCTCGCATGTCTCGTGGGCTCGG
N723	CAAGCAGAAGACGGCATACGAGATGAGCGCTAGTCTCGTGGGCTCGG
N724	CAAGCAGAAGACGGCATACGAGATCGCAGTGTCTCGTGGGCTCGG
N726	CAAGCAGAAGACGGCATACGAGATGTCTAGGTCTCGTGGGCTCGG
N727	CAAGCAGAAGACGGCATACGAGATACTGATCGGTCTCGTGGGCTCGG
N728	CAAGCAGAAGACGGCATACGAGATTAGCTCGCATCTCGTGGGCTCGG
N729	CAAGCAGAAGACGGCATACGAGATGACGTCGAGTCTCGTGGGCTCGG

1257

1258 Note that because of increased risk of index swapping associated with sequencing amplicons
 1259 on Illumina machines with ExAmp technology (Kinsler et al. 2023), we labeled each sample with
 1260 a unique combination of inline and Illumina indices. This allows for reads associated with index
 1261 swapping due to mis-incorporation of indices or template swapping on the sequencing machine
 1262 to be identified and removed from downstream analysis.

1263

1264 For the second step of PCR, we performed 3 reactions per sample. For each set of the 50 µL
 1265 reactions, we used 45 µL of column purified Step 1 PCR product, 2.5 µL of the designated
 1266 forward Nextera XT Index V2 primer (e.g., N716), 2.5 µL of the designated reverse Nextera XT
 1267 Index V2 primer (e.g., S513), 3 µL of 10mM dNTP (Fisher Scientific #PR-U1515), 1.5 µL of Q5
 1268 polymerase (NEB #M0491L), 30 µL of Q5 buffer (NEB #M0491L), and 65.5 µL of nuclease free
 1269 water. We then ran the following program on the thermocycler to amplify for 20 cycles:

1270

1271 1. 98°C 30s
 1272 2. 98°C 10s
 1273 3. 62°C 20s
 1274 4. 72°C 30s
 1275 5. Repeat steps 2-4 19 times (20 cycles total)
 1276 6. 72°C 3min
 1277 7. Hold at 4 C

1278

1279 We then performed column purification following a similar procedure to the purification from step
 1280 1, eluting instead into 30 µL of nuclease free water.

1281

1282 Following the second step of PCR, in order to further remove any residual ancestral barcode
 1283 that were not digested before PCR amplification, we performed a second round of ApaLI
 1284 digestion, adding 3.5 µL of Cutsmart buffer and 1 µL of ApaLI restriction enzyme (NEB
 1285 #R0507L) to each sample's Step 2 PCR product, digesting for at least 1 hr at 37°C. We then
 1286 performed gel extraction using the GeneJet gel purification kit for each sample, keeping the
 1287 350bp band representing intact barcode sequences. We then quantified the DNA concentration
 1288 for each sample using Qubit HS kit (ThermoFisher #Q32854), pooled such that each sample

1289 was equally represented in the final library, and submitted for sequencing on Illumina
1290 sequencing machines.

1291

1292 Tracking evolution

1293 To track the dynamics of the evolution experiment, estimate the fitness of lineages during the
1294 evolution experiment, and infer the distribution of fitness effects, we extracted DNA and used
1295 PCR amplification to generate libraries for sequencing as described above, with the exception of
1296 not performing the ApaLI restriction digestion.

1297

1298 In order to identify barcode counts over time, we followed previously used custom scripts along
1299 with bartender (https://github.com/Sherlock-Lab/Barcode_seq/blob/master/bartender_BC1_BC2.py) to extract and cluster barcodes from
1300 timepoints along the evolution trajectory.

1301

1302 To infer fitness effects, the mean fitness of the population, and infer the from the evolution
1303 experiments themselves, we used FitMut1 (Levy et al. 2015; F. Li, Mahadevan, and Sherlock
1304 2023). To infer the distribution of fitness effects from this data, we used an approach developed
1305 in Levy et al 2015. The general idea of this approach is to infer the distribution of fitness effects
1306 by counting the number of mutants arising with selection coefficients in the interval [s, s+ds]
1307 across the course of the evolution experiment. To infer a rate, we adjust the amount of time that
1308 this mutant could have arisen and been detected based on the mean fitness of the population,
1309 the time it takes for the mutant to establish, and its ability to rise to a detectable frequency in the
1310 population. Specifically, the number of mutations in the interval [s, s+ds] is expected to be:

$$1313 \text{number of mutations in } ds = \mu(s)ds \times (s/c) \times N_e \int_0^{t-(1/s)\ln(n_0s/c)} e^{-\bar{x}(t)}dt$$

1314

1315 Where $N_e = 7 \times 10^7$ is the effective population size, $\bar{x}(t)$ is the mean fitness of the population
1316 over time, c is the offspring number variance, and n_0 is the effective lineage size. We invert
1317 this function to estimate $\mu(s)$.

1318

1319 Counting barcodes and calculating fitness from fitness measurement sequencing data

1320 We used BarcodeCounter2 (Venkataram et al. 2016; *BarcodeCounter2: Count DNA Barcodes*
1321 *Version 2*, n.d.) to assign reads to their associated samples and barcodes. Briefly, we extracted
1322 the inline index, barcode, and UMI regions from each read using BLAST (Altschul et al. 1990) to
1323 the known constraint region in the amplicon sequence. Then, we associated each read to its
1324 corresponding condition and timepoint based on its combination of Illumina and inline indices.
1325 We then used Bowtie2 (Langmead and Salzberg 2012) to map the extracted barcode regions to
1326 our known list of barcodes in the experiment, used UMIs to avoid over-counting duplicate reads,
1327 and counted the number of barcodes per sample.

1329 To infer fitness values, we used the fitness inference procedure as developed previously. In
1330 each time interval, a mutant's fitness is calculated as it's log-frequency change, adjusted by the
1331 mean fitness of the population. We infer the mean fitness of the population by calculating the
1332 log-frequency change of the set of 60 neutral lineages from Venkataram 2016.

1333

1334

1335 **Frequency dependence**

1336 During the analysis of the fitness measurement data, we noticed a systematic shift of fitness
1337 over the course of the experiment, with many barcoded mutants showing a decline in fitness
1338 fitness in 1- and 2-Day experiments as the fraction of the population that was adaptive
1339 increased, even after adjustment for changes in mean fitness (Figure S1). These trends were
1340 not identified in previous experiments, and we suspect that this is due to frequency-dependent
1341 fitness effects driven by the very strongly adaptive mutants. To avoid the influence of these
1342 effects, we used only the first timepoint interval from 2-Day experiments (from timepoint 0 to
1343 timepoint 1), as this kept our fitness measurements consistent with previous studies [cite
1344 Kinsler, Li]. Throughout the rest of the study, 2-Day fitness refers to this measurement using
1345 only early timepoints.

1346

1347 **Quantifying performances**

1348

1349 To quantify mutant performances in each phase of growth, we quantified differences between
1350 fitnesses inferred from 1-, 2-, 3-, and 5-Day transfer experiments. Because the time interval
1351 between 24 and 48 hours only contains respiration phase, we quantified respiration
1352 performance per hour as:

$$1353 \text{ResPerHour} = \text{2-Day fitness} - \text{1-Day fitness} / 24\text{hrs}$$

1354 To calculate fermentation performance, we removed the 4 hours worth of respiration
1355 performance from the 1-Day fitness and divided the remaining fitness into the 16 hours of
1356 fermentation performance (accounting for ~4 hours of lag phase):

$$1357 \text{FerPerHour} = (\text{1-Day fitness} - 4 * \text{ResPerHour}) / 16\text{hrs}$$

1358

1359 Because 1-Day fitness measurements are used for both respiration and fermentation
1360 performances, there is the potential for noise in 1-Day measurements to introduce a relationship
1361 between fermentation and respiration performances. To eliminate measurement noise from
1362 having this influence, we used different replicates of the 1-Day fitness to calculate fermentation
1363 and respiration performance. Specifically, we used the replicate 2 flasks to calculate respiration
1364 performance and the replicate 1 flasks to calculate fermentation performance.

1365

1366 To infer stationary phase performance, we took the difference between 5- and 3-day fitness and
1367 divided by 48hrs of time:

$$1368 \text{StaPerHour} = (\text{5-Day fitness} - \text{3-Day fitness}) / 48\text{hrs}$$

1369

1370 To calculate the uncertainty of performances, we used error propagation from the estimated
1371 errors of fitness. To calculate performances relative to parental strain, we computed the
1372 difference between each mutant's performance and its parental strain. For *CYR1*, *GPB2*, *TOR1*,
1373 and *IRA1-missense* second-step mutations, we used the mean of the neutral barcode strains as
1374 the parental reference measurement. For *IRA1-nonsense* second-step mutations, for which no
1375 neutral clones were isolated, we used the parental barcoded barcoded mutant present in the
1376 pool of first-step mutants (denoted with a "+" in main text figures).

1377

1378 **Differences in selection pressure do not drive the shift towards modular adaptation**

1379

1380 To evaluate whether a systematic shift in selection pressure occurred during the second-step
1381 evolution experiments, we identified mutants for which we called their evolution fitness from the
1382 estimation of the distribution of fitness effects. Because many of the remaining mutants are pure
1383 diploids whose spread may be dominated by measurement noise, we removed these mutants
1384 from the list. This resulted in a set of 185 second-step mutants. We then performed a partial
1385 correlation analysis between respiration performance and evolution fitness, accounting for
1386 fitness measurement fitness. We find no evidence of such a relationship ($p=0.74$, $r=-0.02$).
1387 Similarly, we find no relationship between fermentation performance and evolution fitness after
1388 accounting for fitness measurement fitness ($r=0.38$, $p=0.613$).

1389

1390 **1-Day evolution experiment analysis**

1391

1392 To evaluate whether yeast adapting to a 1-Day transfer could further improve their fermentation
1393 performance, we quantified the performance of 1-Day mutants as above. We identified several
1394 mutants with fermentation performances meeting or exceeding the maximum fermentation
1395 performance achieved by first-step mutants. Using a threshold of at least 2 standard errors
1396 (which corresponds to a FDR of $p<0.05$) a single second-step mutant that arose in the Evo1D
1397 *IRA1-nonsense* population had fermentation performance that exceeded the first-step
1398 maximum.

1399

1400 **Whole genome sequencing**

1401 We selected mutants for whole genome sequencing based on their fitness and performance in
1402 the growth phase, such that we selected as many unique mutants as possible based on their
1403 performances and those that had barcodes confidently identified by the metagrid. This resulted
1404 in a total of 346 clones targeted for sequencing.

1405

1406 Clones that were selected for sequencing were grown in 500 μ L of YPD in 96-well deep well
1407 plates for 2 days at 30°C without shaking. 400 μ L of saturated culture was collected from each
1408 well for genomic DNA extraction using the Invitrogen PureLink Pro 96 Genomic DNA Kit.
1409 Libraries were prepared using a $\frac{1}{5}$ dilution protocol of the Illumina DNA prep, using Illumina
1410 Unique Dual Indexing primers.

1411

1412 **Variant calling**
1413 To identify variants from the sequencing data, we used bwa (H. Li and Durbin 2009) to align all
1414 reads to the S288C reference genome (R64-1-1-20110203). We then used picard
1415 (<https://broadinstitute.github.io/picard/>) to fix read groups and mark duplicate reads. We then
1416 used GATK (version 4.2.0.0) (Van der Auwera and O'Connor 2020) to generate individual
1417 GVCF files, merge GVCF files, and call genotypes on all samples. After removing samples with
1418 less than 20x coverage, we removed variants according to the following filters: QD < 5, FS < 60,
1419 SOR < 3, M! < 50, MQRankSum < -3.0, ReadPosRankSum < -5.0. After this filtering, we further
1420 removed ancestral variants present in all samples, mitochondrial variants, variants with GQ less
1421 than 70. This filtering resulted in 727 sites that were variable across our samples. We then
1422 manually inspected all called variants, resulting in 631 manually verified variants. We then used
1423 bcftools (H. Li 2011) to filter the vcf file to these verified variants and used snpEff (Cingolani et
1424 al. 2012) to annotate variants.

1425
1426 We then assigned variants to the corresponding barcoded mutants based on plate position. To
1427 check that our assignment was correct, we also verified the barcodes from the whole genome
1428 sequencing reads. For the 326 mutants for which we had sufficient coverage of the barcode
1429 region (at least 4 successfully-mapped barcode reads), 324 had the correct barcode identified.
1430 We opted to not use sequencing information from the 2 samples with mismatching barcodes
1431 between the sequencing and expected based on clone isolation barcode sequencing.

1432
1433 We further identified pre-existing mutations in which identical mutations were present in several
1434 sequenced mutants of a given low-complexity barcode. These mutations were classified as
1435 “pre-existing” mutations and ignored in downstream analyses except in cases where they
1436 belonged to a putatively causal gene (see “Mutation and ploidy classification” section).

1437
1438 **Mutation and ploidy classification**
1439

1440 To identify mutations likely responsible for driving fitness gains in these experiments, we
1441 identified putative adaptation-driving mutations by identifying mutations that occurred in genes
1442 that were recurrently mutated across adaptive clones. Specifically, genes with 4 or more
1443 mutations were classified as likely adaptation-driving. After classifying genes based on their
1444 function, we further identified additional mutations as adaptation-driving due to their effect on
1445 similar processes as recurrently mutated genes.

1446
1447 To classify the ploidy of mutations, we initially classified mutants according to their performance
1448 in the benomyl assay. We additionally classified mutants as “pure diploids” and “neutral
1449 haploids” by their similarity to the large cluster of haploids and diploids in terms of their fitness
1450 effects across all the conditions. Mutants that were within this large cluster of diploids but initially
1451 classified as haploids according to the benomyl assay were classified as pure-diploids.

1453 From this initial ploidy classification, the majority of mutants which exhibited mutations in *PAB1*
1454 were classified as diploids, perhaps reflecting a sensitivity of *PAB1* mutants to benomyl. We re-
1455 classified all *PAB1* mutants as adaptive haploids with respiration performance relative to
1456 parental strain less than 0.06. *PAB1* mutants with greater respiration performance were
1457 classified as high-fitness diploids, consistent with the effect that auto-diploidization had on
1458 mutations from other genes. Similarly, *PAN2* and *PAN3* mutants were classified as diploids and
1459 have previously been shown to be susceptible to benomyl (Brown et al. 2006). Given we had
1460 few of these mutations, we did not have enough information to reclassify these mutations as we
1461 did for *PAB1*.
1462

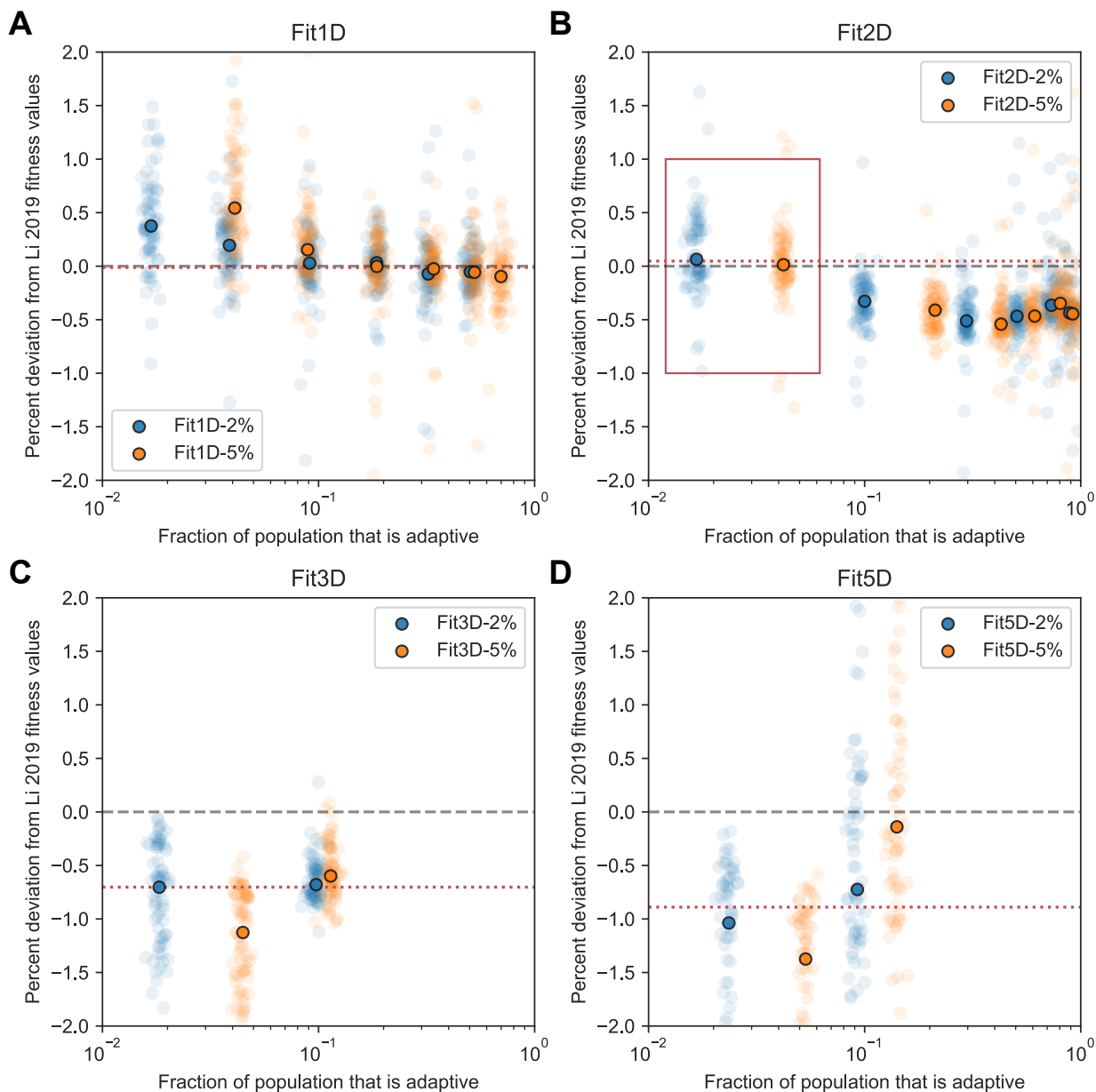
1463 **Data availability**

1464 Raw sequencing data is available on Short Read Archive under BioProject Number:
1465 PRJNA1098711. Processed frequency counts, fitness data, performance data, and mutational
1466 calls are available on Github: <https://github.com/grantkinsler/EvolvingFront>. All yeast strains are
1467 available upon request.

1468

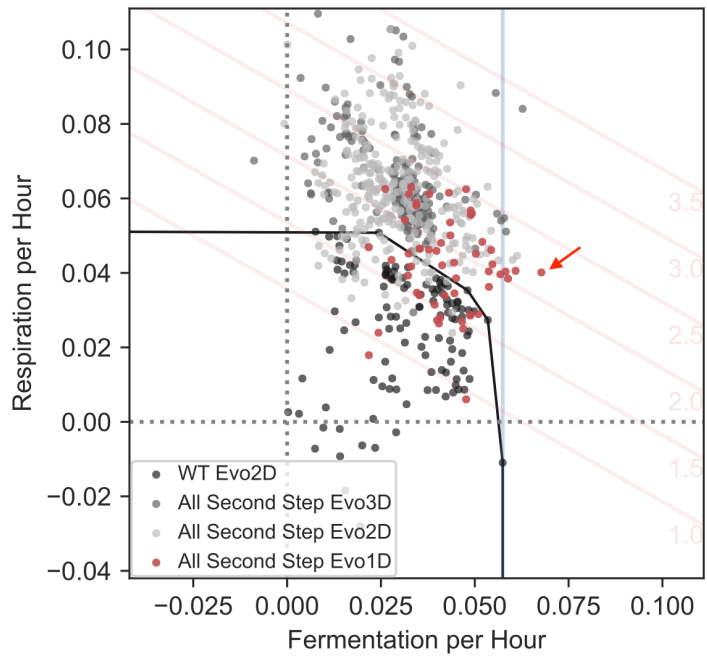
1469 **Code availability**

1470 Code for all data processing and figure generation is available on Github:
1471 <https://github.com/grantkinsler/EvolvingFront>

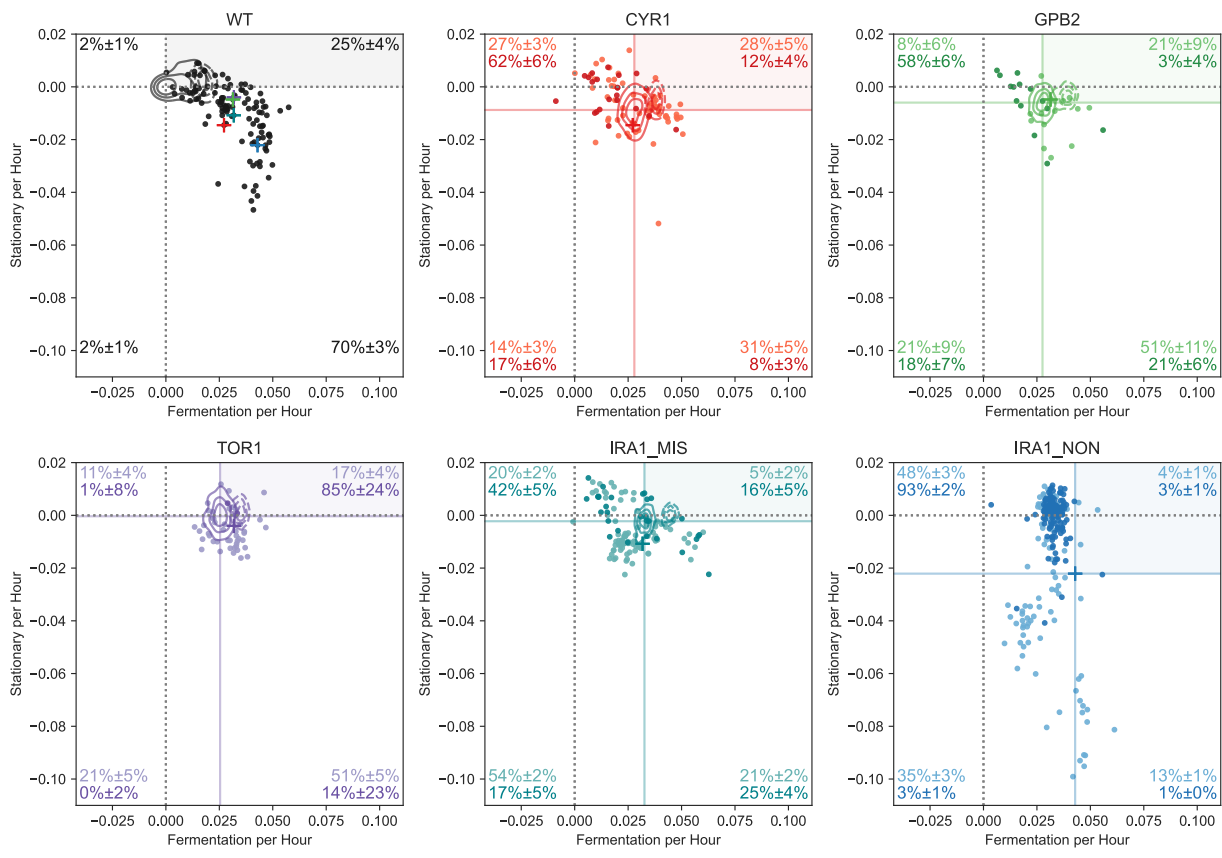
1472 **SUPPLEMENTARY FIGURES**

1473

1474 **Fig S1. Evidence for frequency dependence in fitness measurement experiments.** The
 1475 vertical axis of each subplot depicts the percent deviation from Li 2019 fitness values for the set
 1476 of adaptive haploids that were present in Li 2019 fitness measurements and this study. The
 1477 horizontal axis is the fraction of the population that is adaptive. Points show the deviation for
 1478 each mutant, with the median across all mutants depicted by the heavy circle. Blue and orange
 1479 points are from experiments initiated with the adaptive barcode pool consisting of 2% and 5% of
 1480 the population, respectively. Red dotted line indicates the deviation for the overall fitness
 1481 measurement used throughout the paper. Red box in (B) refers to the timepoints used.
 1482 Subpanels A-D refer to Fit1D, Fit2D, Fit3D, and Fit5D fitness values, respectively.



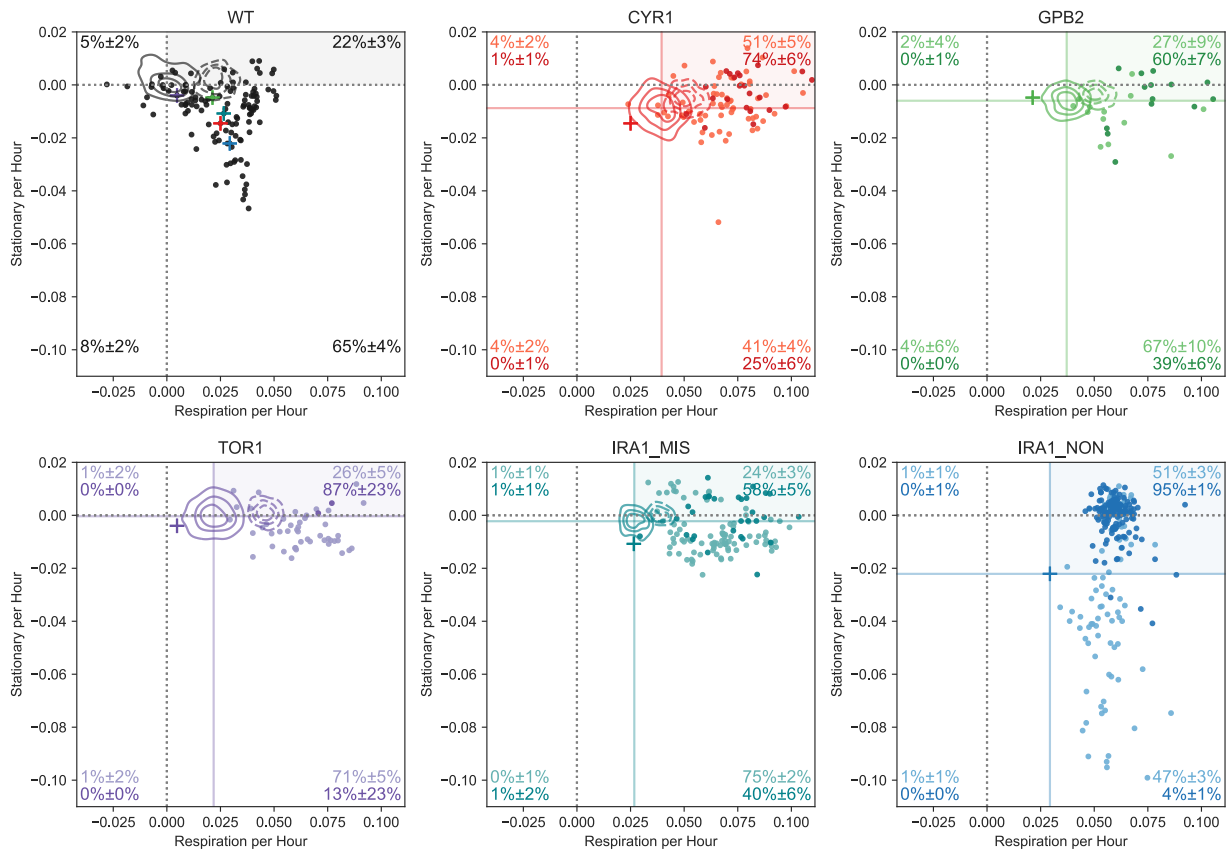
1483 **Fig S2. 1-Day evolution experiments identify mutants that improve fermentation**
 1484 **performance.** Fermentation and respiration performances for mutants discussed in the main
 1485 text and Evo1D mutants (in red). Despite less dense sampling, we find at least one Evo1D
 1486 mutant (indicated with red arrow) with fermentation performance that exceeds the highest
 1487 fermentation performance from first-step mutants (blue vertical line).



1488

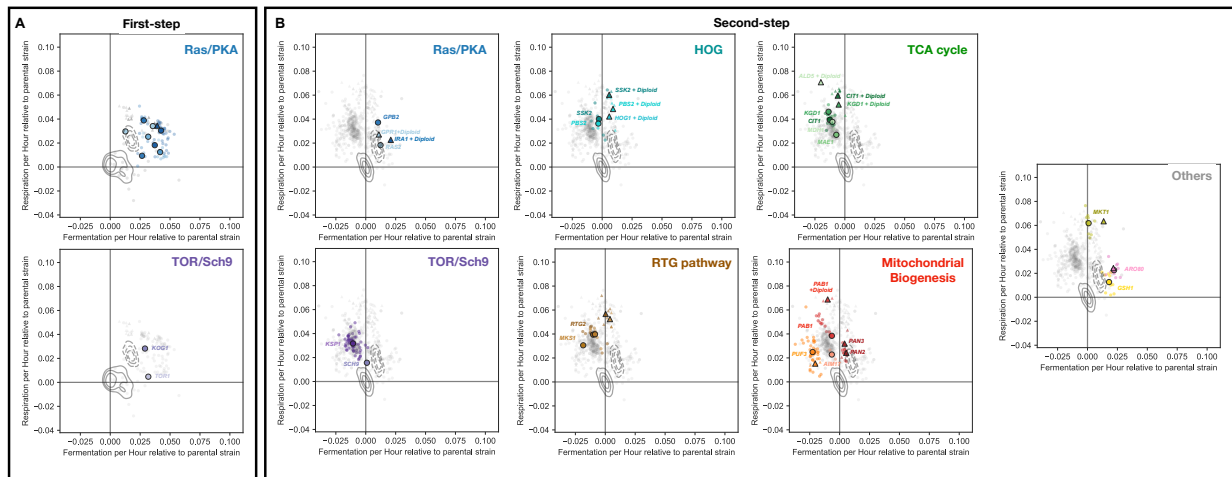
1489

Fig S3. Fermentation and stationary phase performances by parental strain. Each
1490 subpanel depicts a scatter plot with the fermentation and stationary performances for each
1491 parental strain. Lighter points indicate Evo2D mutants, darker points indicate Evo3D mutants.



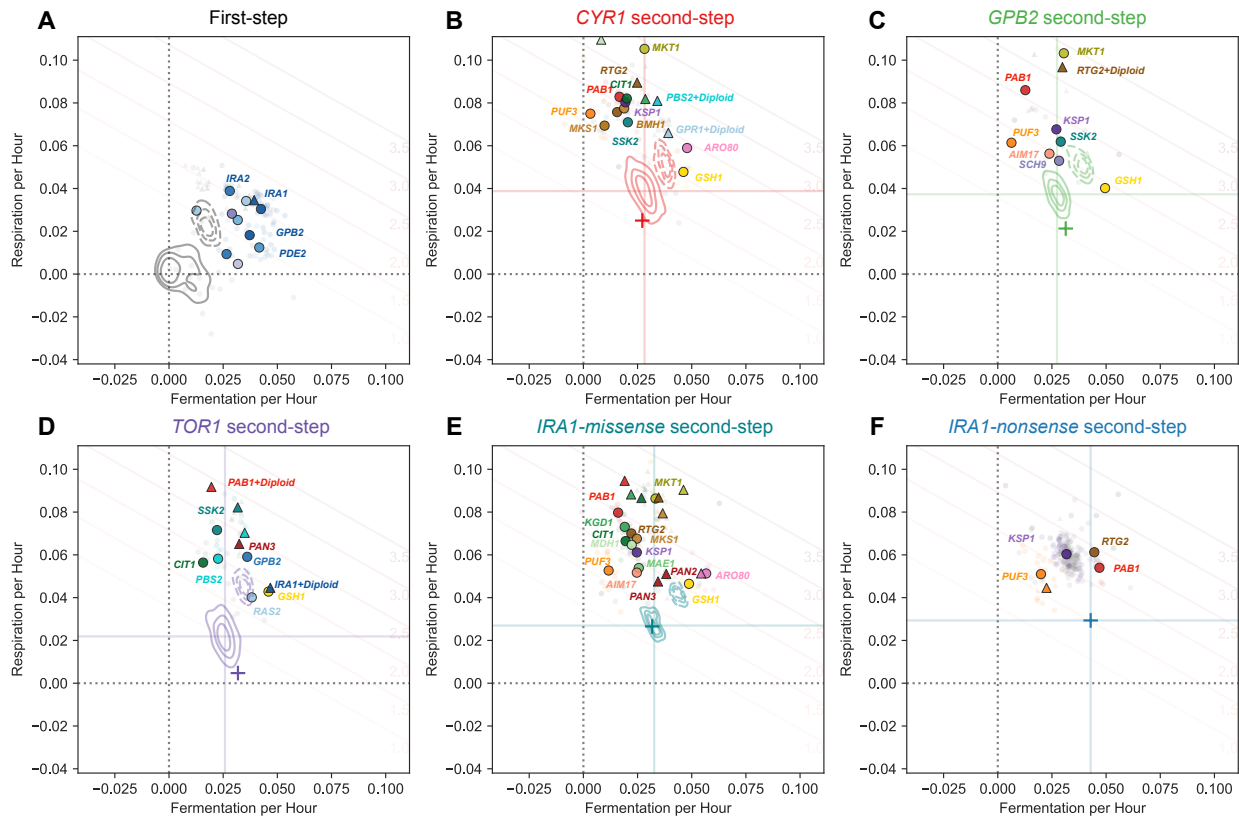
1492
1493
1494
1495

Fig S4. Respiration and stationary phase performances by parental strain. Each subpanel depicts a scatter plot with the respiration and stationary performances for each parental strain. Lighter points indicate Evo2D mutants, darker points indicate Evo3D mutants.



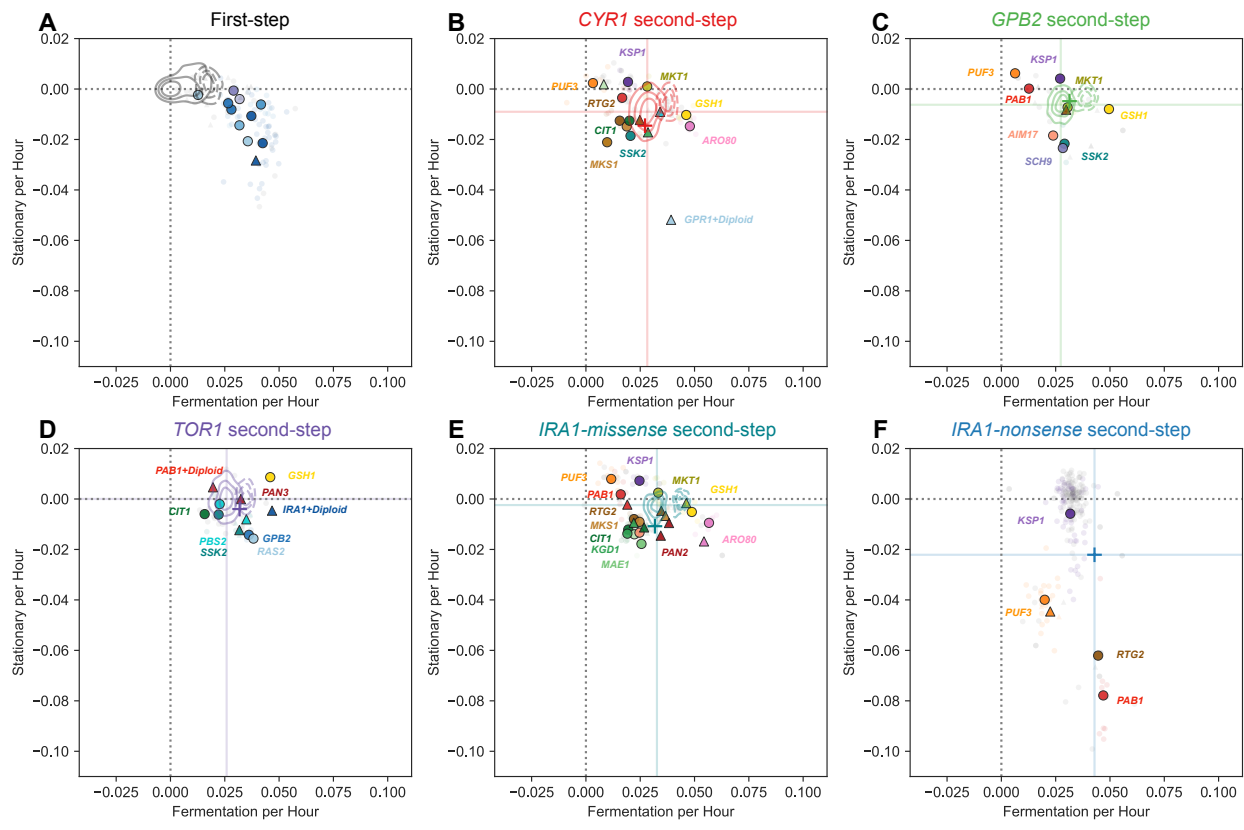
1496
1497
1498
1499
1500
1501
1502

Fig S5. Molecular targets of adaptation by gene. Performance effects of mutations separated by biological process or pathway as in Table 1. Points are colored by gene, and shape indicates ploidy (circles are haploids, triangles diploids). KDE estimates show density of neutral haploids for each parental strain (solid lines) and pure diploids for each parental strain (dashed lines). **(A)** First-step mutants. **(B)** Second-step mutants depicted, with performances measured relative to parental strain.

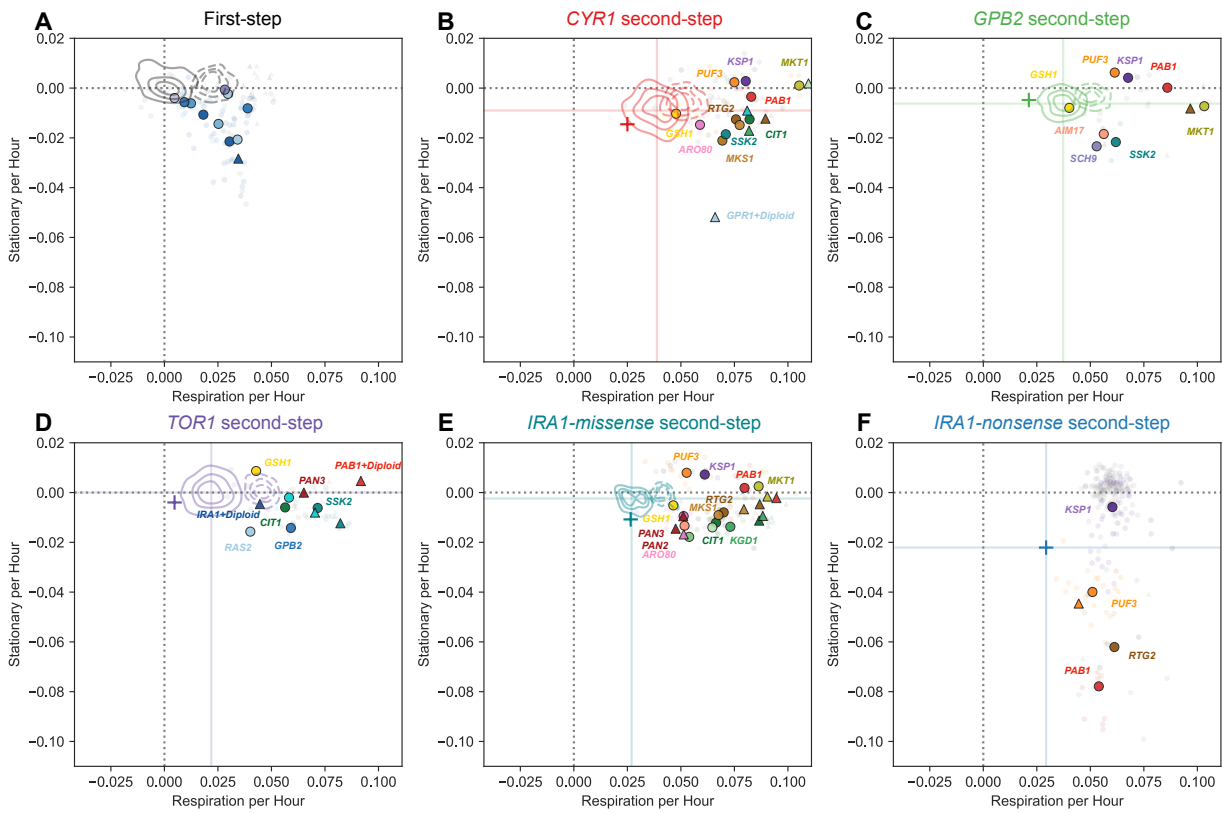


1503
1504
1505
1506

Fig S6. Molecular targets of adaptation by gene. Colored by gene, shape depicts ploidy (circles are haploids, triangles diploids). KDE estimates show density of neutral haploids for each parental strain (solid lines) and pure diploids for each parental strain (dashed lines).



1507
 1508 **Fig S7. Mutational effects on fermentation and stationary phase performance.** Colored by
 1509 gene, shape depicts ploidy (circles are haploids, triangles diploids). KDE estimates show
 1510 density of neutral haploids for each parental strain (solid lines) and pure diploids for each
 1511 parental strain (dashed lines).



1512
1513
1514
1515
1516

Fig S8. Mutational effects on respiration and stationary phase performance. Colored by gene, shape depicts ploidy (circles are haploids, triangles diploids). KDE estimates show density of neutral haploids for each parental strain (solid lines) and pure diploids for each parental strain (dashed lines).